INVESTIGATING FAULT CONTROL ON RESERVOIR ACCUMULATION AND SPATIAL DISTRIBUTION USING 3D SEISMIC DATA AND WELL LOGGING DATA: A CASE STUDY FROM THE LOWER OLIGOCENE VICKSBURG FORMATION, BROOKS COUNTY, TEXAS

A Thesis

by

RYAN L. TURNER

BS, Texas A&M University-Corpus Christi, 2018

Submitted in Partial Fulfillment of the Requirements for the Degree of

MASTER OF SCIENCE

in

COASTAL AND MARINE SYSTEM SCIENCE

Texas A&M University-Corpus Christi
Corpus Christi, Texas

December 2020

December 2020

INVESTIGATING FAULT CONTROL ON RESERVOIR ACCUMULATION AND SPATIAL DISTRIBUTION USING 3D SEISMIC DATA AND WELL LOGGING DATA: A CASE STUDY FROM THE LOWER OLIGOCENE VICKSBURG FORMATION, BROOKS COUNTY, TEXAS

A Thesis

by

RYAN L. TURNER

This thesis meets the standards for scope and quality of
Texas A&M University-Corpus Christi and is hereby approved.

Mohamed Ahmed, PhD
Chair

Richard Coffin, PhD
Committee Member

Lindsay Prothro, PhD
Committee Member

Mr. Randy Bissell
Committee Member

December 2020

ABSTRACT

In southern Brooks County, Texas, the Lower Oligocene Vicksburg Formation (LOVF, Rupelian stage, approximately 33.9-27.82 million years ago), is being influenced by the Vicksburg Fault Zone (VFZ). The VFZ is characterized by listric-normal faults that have formed highly faulted rollover anticlines that are sought-after structural traps for hydrocarbon exploration. This research explored how secondary synthetic (dipping East), antithetic (dipping West), and coast-perpendicular faults are affecting the accumulation and spatial distribution of hydrocarbons within the La Rucias Field. Results indicate that synthetic, antithetic, and coast-perpendicular faults affecting the V-102, V-17, and V-19 horizons provide conduits for hydrocarbon migration. Antithetic faults and coast-perpendicular faults within the rollover anticline are terminating beneath the overlying shale seal layer between the V-16 and V-17, creating natural gas accumulation. While synthetic faults affect the overlying seal layer migrating gas out of the V-102, V-17, and V-19. Bidirectional faulting linking antithetic and perpendicular to the coast faults are acting as additional pathways for enhanced hydrocarbon accumulation. Spatial distribution of hydrocarbons within the La Rucias Field varies with the horizon being targeted. Productive V-102 reservoirs are located on the western flank of the rollover anticline, the V-17 and V-19 reservoirs are located on structural highs where antithetic faults are not affecting the overlying shale seal layer, and the most productive V-17 and V-19 reservoirs are being affected by bidirectional faulting terminating beneath the shale seal layer allowing accumulation and spatial distribution within the rollover anticline. Investigating the control of these fault systems enhances our understanding on subsurface fluid migrations and accumulations (oil, gas, groundwater, and contaminants) in the expanded Vicksburg productivity trends.

DEDICATION

This thesis is dedicated to my grandparents (Robert and Marian Lewis), (Robert and Mary Jane Turner), my aunt (Lisa Turner), to my parents (Robert Turner and Lesley Perry), and to my entire family and friend group for their endless love and support.

ACKNOWLEDGEMENTS

I would like to thank my thesis committee for their continued support and efforts, as well as their advice and guidance throughout this research project. In particular, Dr. Mohamed Ahmed and Randy Bissell for their support and endless feedback throughout the research and writing process. I would like to thank Dr. Coffin and Dr. Prothro for the feedback and support throughout the project. I would also like to thank Dawn Bissell for her guidance and tutelage during the research and interpretation processes. Additionally, I would also like to thank Petrophysics, Inc. for their generous donation of a velocity and sonic survey, the Corpus Christi Geological Library for their generous donation of well logs and production data, and Seismic Exchange, Inc. for their donation of a 2D seismic line.

TABLE OF CONTENTS

LIST OF FIGURES

FIGURES PAGE

LIST OF TABLES

TABLES PAGE

CHAPTER I

Introduction

Overview

The Lower Oligocene Vicksburg Formation (LOVF) in southern Brook County Texas is a highly productive natural gas reservoir system with alternating paralic/deltaic sand and marine shale intervals (Whitbread et al., 2001). The LOVF is being influenced by the Vicksburg Fault Zone (VFZ). Listric normal faults, oriented parallel to the Texas Gulf Coast, have developed highly complex secondary faulted rollover anticlines within the VFZ (Combes, 1993). These geologic structures, among others, are affecting the LOVF reservoir accumulation and spatial distribution of hydrocarbon productivity.

The LOVF within the Coastal Plains of Texas is an economically important formation, specifically within the Rio Grande Embayment (Combes, 1993). The purpose of investigating fault control within the LOVF is to better assess vertical compartmentalization of reservoir intervals, accumulation, and resolve the spatial distribution of hydrocarbons within the La Rucias Field. The La Rucias is a natural gas field located within the study area. Exploring the control of these secondary fault systems also enhances our understanding of subsurface fluid (oil, gas, groundwater, and contaminants) behavior in Coastal Bend listric normal fault systems as well as other gravity driven basins.

To investigate the effects of fault control on the LOVF reservoir, a post-stack 3D seismic dataset was integrated with available well logging data (39 well logs; spontaneous potential [SP], gamma ray [GR], resistivity, and sonic) and three velocity surveys. The following tasks and objectives have been accomplished. (1) Explore fault control by mapping seismic horizons

Vicksburg Top (VX-Top), V-14, V-15, V-16, V-102, V-17, and V-19 as well as faults affecting these horizons; (2) construct two-way travel time (TWT) maps for the mapped horizons, (3) produce structural depth maps by converting time to depth using the available velocity surveys, and (4) construct a comprehensive conceptual model to explain the effects of faults on the accumulation quality and spatial distribution of hydrocarbons within the LOVF.

Study Area

The study area is located within southern Brooks County, Texas (Figure 1). We are targeting the southern La Rucias Field (Carter Ranch Lease) that is located south of the northern

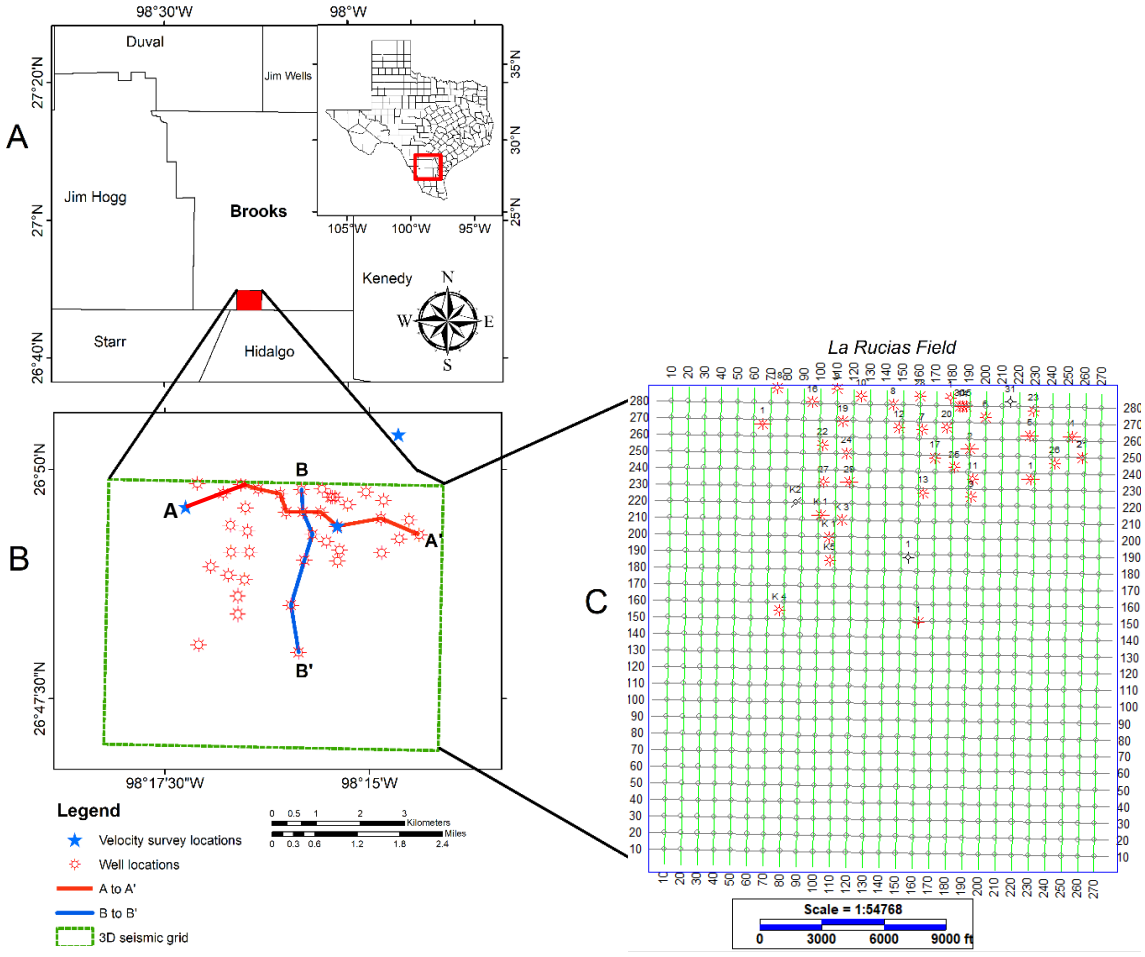

Figure 1: (A): Location of study site within southern Brooks county, Texas. (B): Map showing the outline of the 3D seismic grid, location of velocity surveys, location of wells, and cross sections A to A' and B to B'. (C): The 3D seismic grid with well locations within the La Rucias Field.

La Rucias Field (Lopez Ranch Lease). Within the VFZ, over 373 fields were reported to produce from the Vicksburg Formation (Coleman et al., 1990).

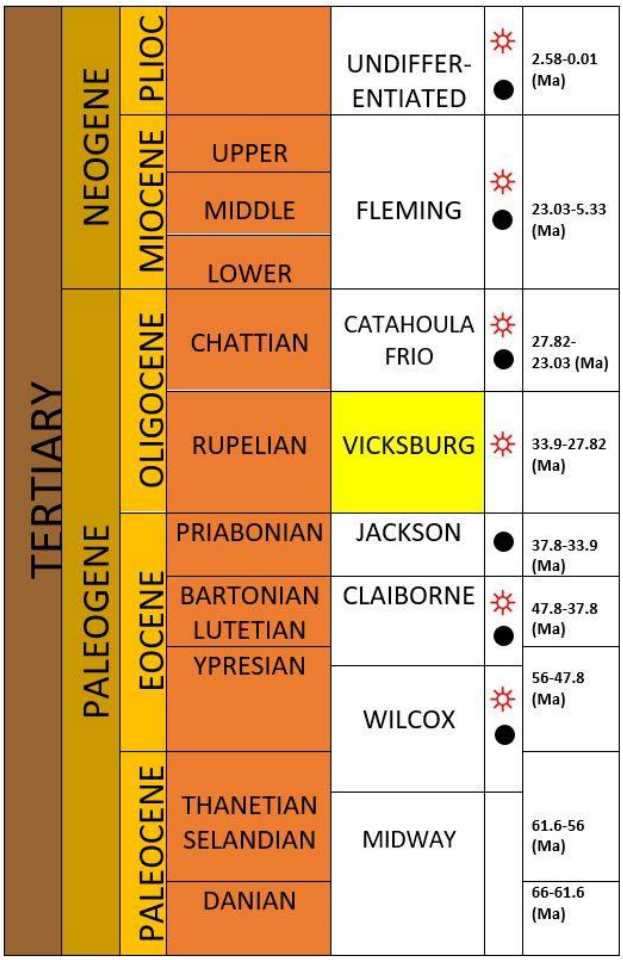

Figure 2: Stratigraphic column of the study area.
The Vicksburg Formation is highlighted in yellow.

The Lower Oligocene Vicksburg Formation is a highly faulted, largely extensionally complex, time-transgressive lithostratigraphic unit that spans the northern Gulf of Mexico and Coastal Plains region of Texas. The LOVF (Rupelian stage, approx. 33.9-27.82 Ma), confirmed by bio stratigraphic index fossils (Saito et al., 1964) overlies the Eocene Jackson Formation and underlies the Upper Oligocene Frio-Catahoula Formation, all of which are part of the Tertiary depositional wedge (Figure 2; Coleman et al., 1990). Due to volcanic sediment influx within the

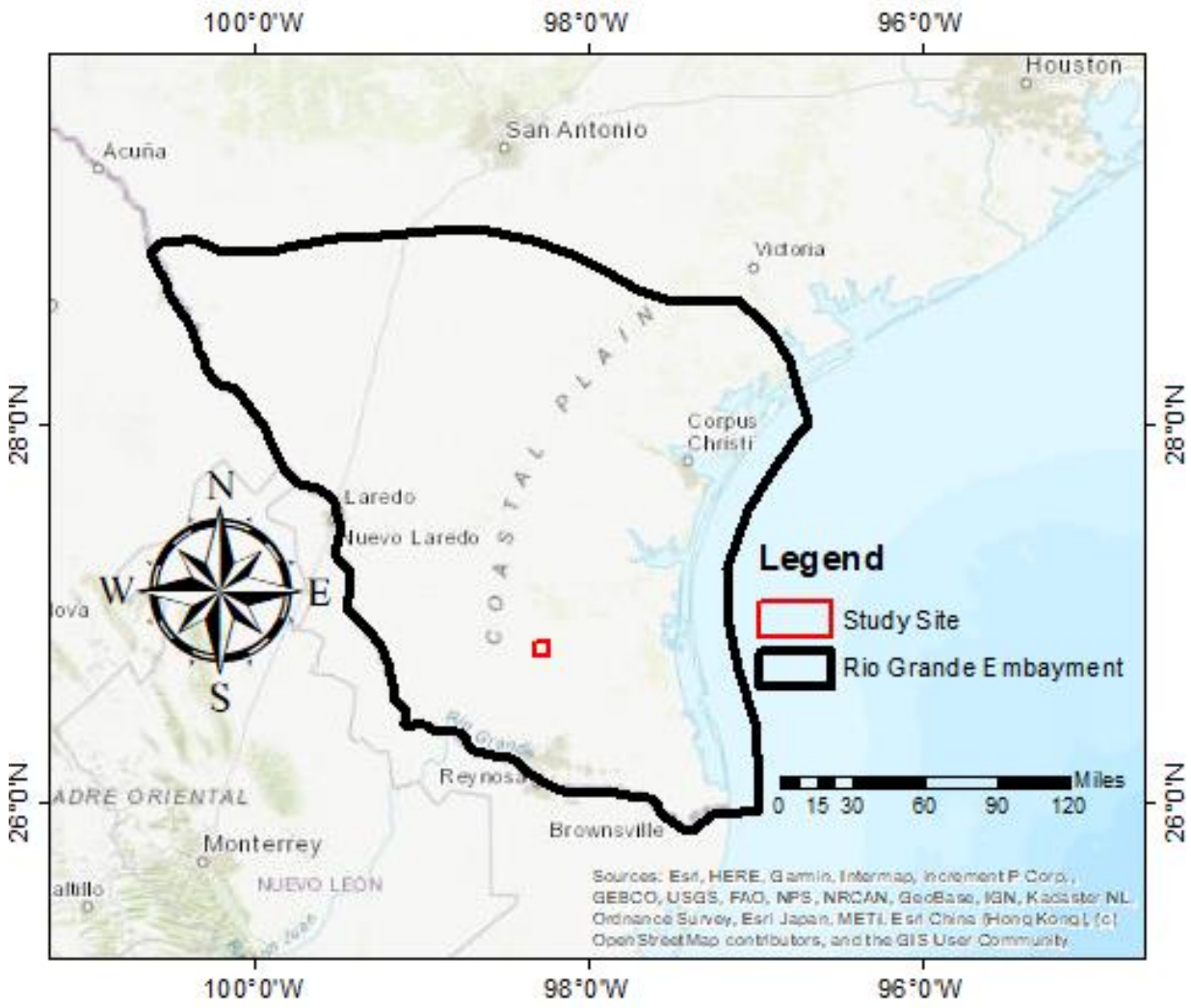

Figure 3: The spatial distribution of the RGE. The study area is shown as a red square. The background image is provided by ESRI.

Rio Grande Embayment (RGE) during the Oligocene Epoch (Figure 3), the VFZ trend is dynamic in hydrocarbon accumulation and faulted structures are complex (Combes, 1993; Salvador, 1991). The extensive deposition within the RGE is attributed to the high sedimentation rates from the eroded volcanic sediment (Combes, 1993; Salvador, 1991). The structural style of the RGE includes coast-parallel synthetic and antithetic faults. The geometry of these faults alternates from coast-perpendicular shale ridges, sub basins, and coast-perpendicular faults, indicating vertical loading and lateral compression causing rollover anticlines to form that show a generally north-

east to south-west trend (Ogiesoba et al., 2018). This fault zone stretches from Mexico to the north east-coast of Texas, parallel to the strike of the depositional basin (Salvador, 1991). The extensional nature of faulting is due to many factors: the influx of sediments, a low stand systems tract, subsidence of differential overburden, shear stress overcoming compressional stress, gravity spreading, and shale diapirism (Brown et al., 2004; Coleman et al., 1990; Han, 1980; Treviño et al., 2008). During the Rupelian stage of the Oligocene, overburden particularly of the mobile Jackson Shale caused listric faults to form subparallel to the Texas coastline. The LOVF was deposited during the Lower Oligocene Epoch, a period that is characterized by extensive volumes of prograding shelf-edge deltaic deposits along the ancient coastline of Texas. The Vicksburg

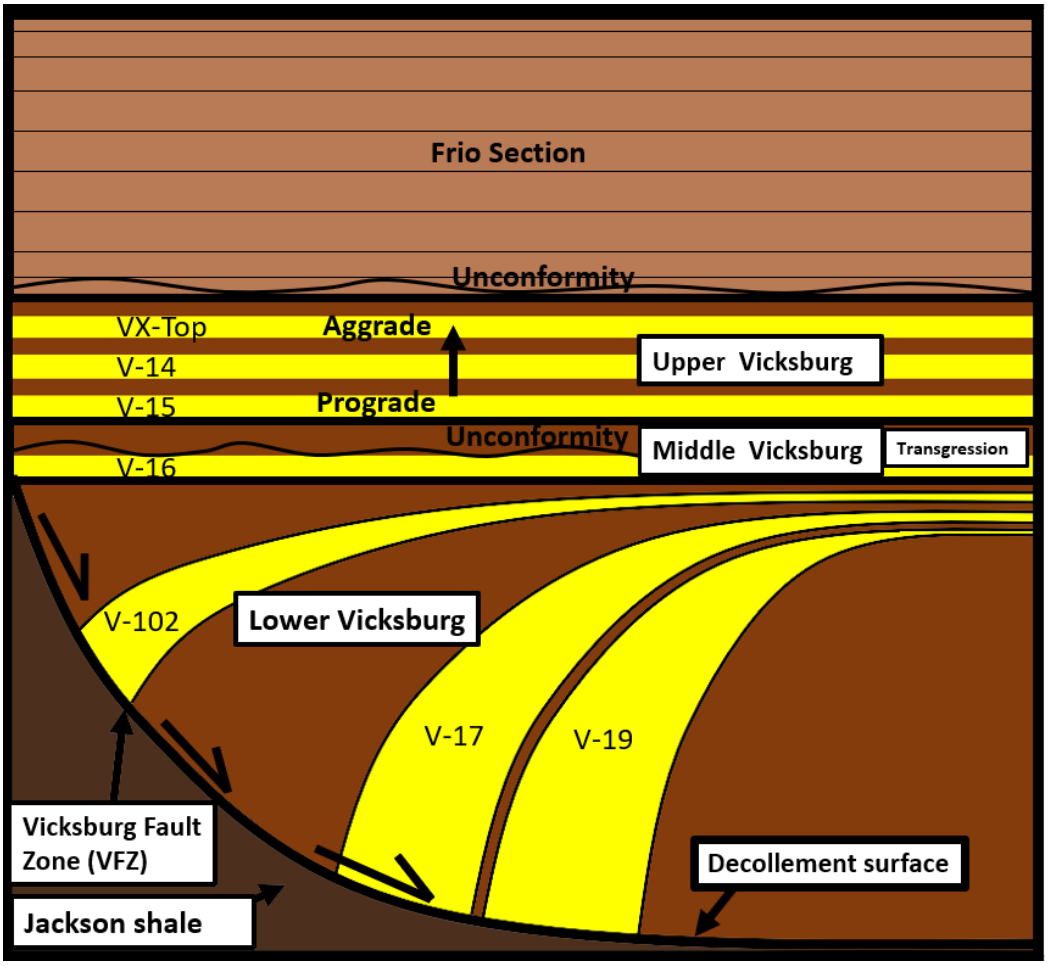

Figure 4: Schematic cross section showing the upper, Middle, and Lower Vicksburg units. Sand units are colored in yellow and shales are shown in brown colors.

Formation is subdivided into Lower, Middle and Upper sections (Coleman et al., 1990; Combes, 1993; Whitbread et al., 2001) (Figure 4). The Lower section of the Vicksburg Formation is a shore-zone complex that is interpreted to be a sand-abundant interdeltaic strand line with a north-northeast strike (Combes, 1993). The Middle section is marked by a transgressive series of backstepping parasequences. The Upper section is defined by an influx of sediment then a change from progradational deposits to the aggradational Frio Formation (Posamentier et al., 1988).

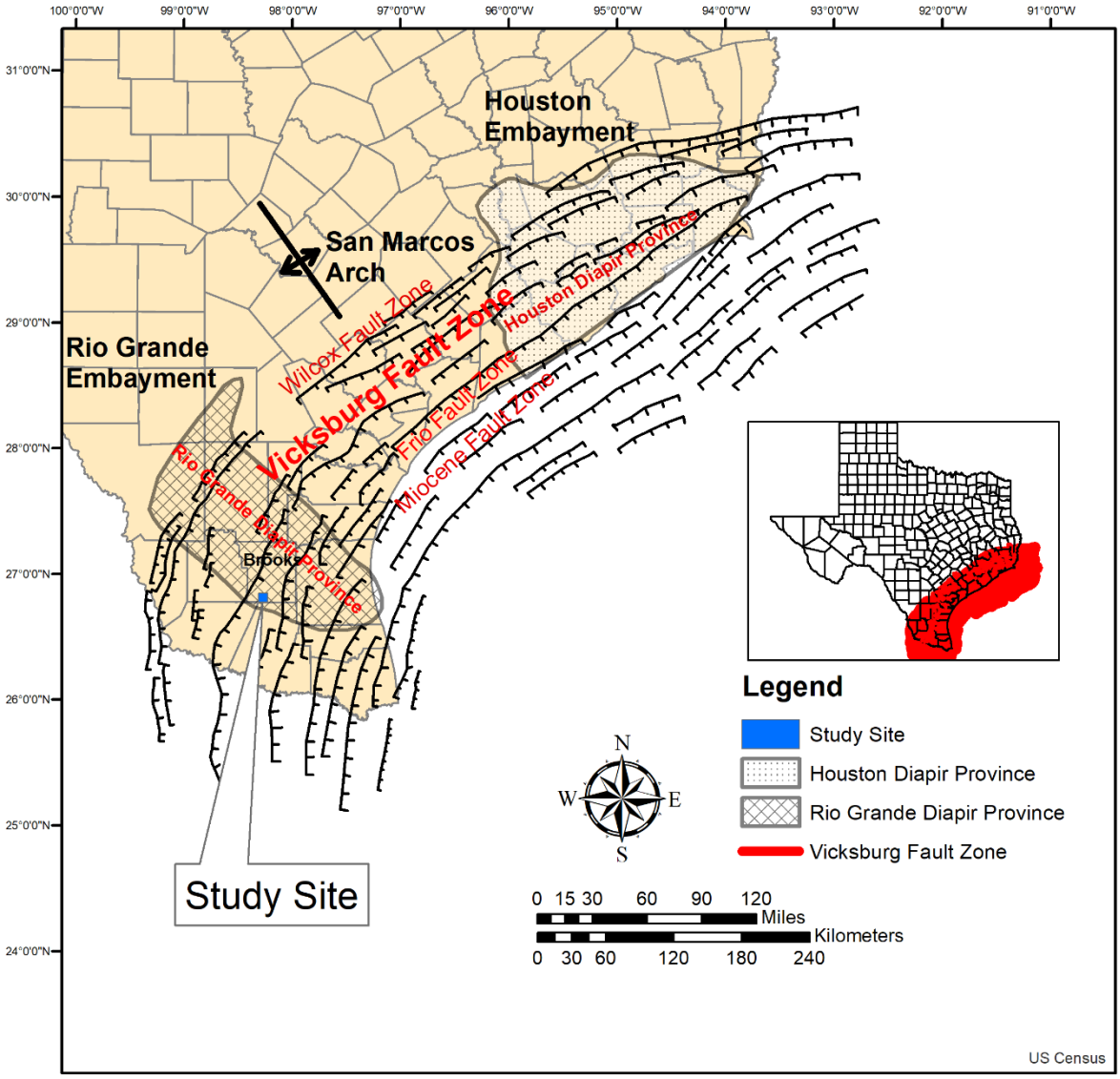

Figure 5: Map showing fault zones and sedimentary basins in Coastal Texas. Study area shown in red square. Modified from (Reeher, 2017, Ewing, 1991; Kosters et al., 1989).

Listric normal faults affecting the LOVF (Figure 5) in southern Brook County Texas, developed from a combination of deposition of deltaic/paralic sand above unconsolidated relic shelfal sediments (Jacksons Shale), gravity tectonics, and a low stand systems tract. Low-stand depocenters up dip from upper continental slopes, with prograding deltaic systems provide the overburden needed to initiate gravitational movement basinward towards the Gulf of Mexico

(GOM) (Brown et al., 2004). This instability developed largely coast parallel, listric normal faults extending towards the GOM. The relative fall in sea level, influx of volcanic sediments from western Texas, and gravity tectonics during the Rupelian stage of the Oligocene triggered major regional syndepositional faulting affecting the LOVF, producing the VFZ stretching from the RGE across the San Marcos Arch into to the Houston Embayment (Figure 5).

The VFZ typically forms basinward-dipping listric faults and associated fault-bend folded rollover anticlines (Figure 4). The critical slope angle to initiate gravity spreading depends on the shear strength of the source layer. These values are similar to measurements of bathymetric slopes found in passive margins such as the GOM (Gaullier et al., 2005). As the listric fault rotates it becomes almost parallel with the Eocene Jackson Shale glide plane. The true dip most likely never exceeds 3° (Whitbread et al., 2000). The VFZ is composed of a stacking sequence of displaced detachments that dip towards the coast and are affected by the synthetic and antithetic secondary faults.

Fault zones have the capacity to provide gas and fluid conduits linking deep and shallow geologic units (Bense et al., 2013). Faults can also exhibit sufficient throw to displace sand-shale units to act as barriers to fluid flow. Connectivity of faulted reservoirs is controlled by several parameters, such as thickness and net gross of the faulted intervals (V-102, V-17 and V-19), size, dimensionality, and the distribution of reservoir units (Bailey et al., 2002). Additionally, the gross ratio of sand to shale may affect fault effectiveness due to fault gouge. Vertical displacement along listric normal faults is influential in developing structural traps such as rollover anticlines and horst blocks (Bose et al., 2012; Shelton, 1984). Rollover anticlines in ancient deltaic environments usually form asymmetrical antiforms, where the sedimentary units thicken distinctively towards

the basinward-dipping master fault (e.g., VFZ) (Fazli et al., 2015). Faulting in the VFZ is syndepositional and the deeper horizons in the lower Vicksburg (V-102, V-17 and V-19) were rotated to form structural highs (Berg et al., 1982). Complex growth fault zones associated with rollover anticlines provide prolific fault trap opportunities (Figure 6) (Brown et al., 2004). As exploration moves toward more complex areas of interest, through evaluation of the role of fault-

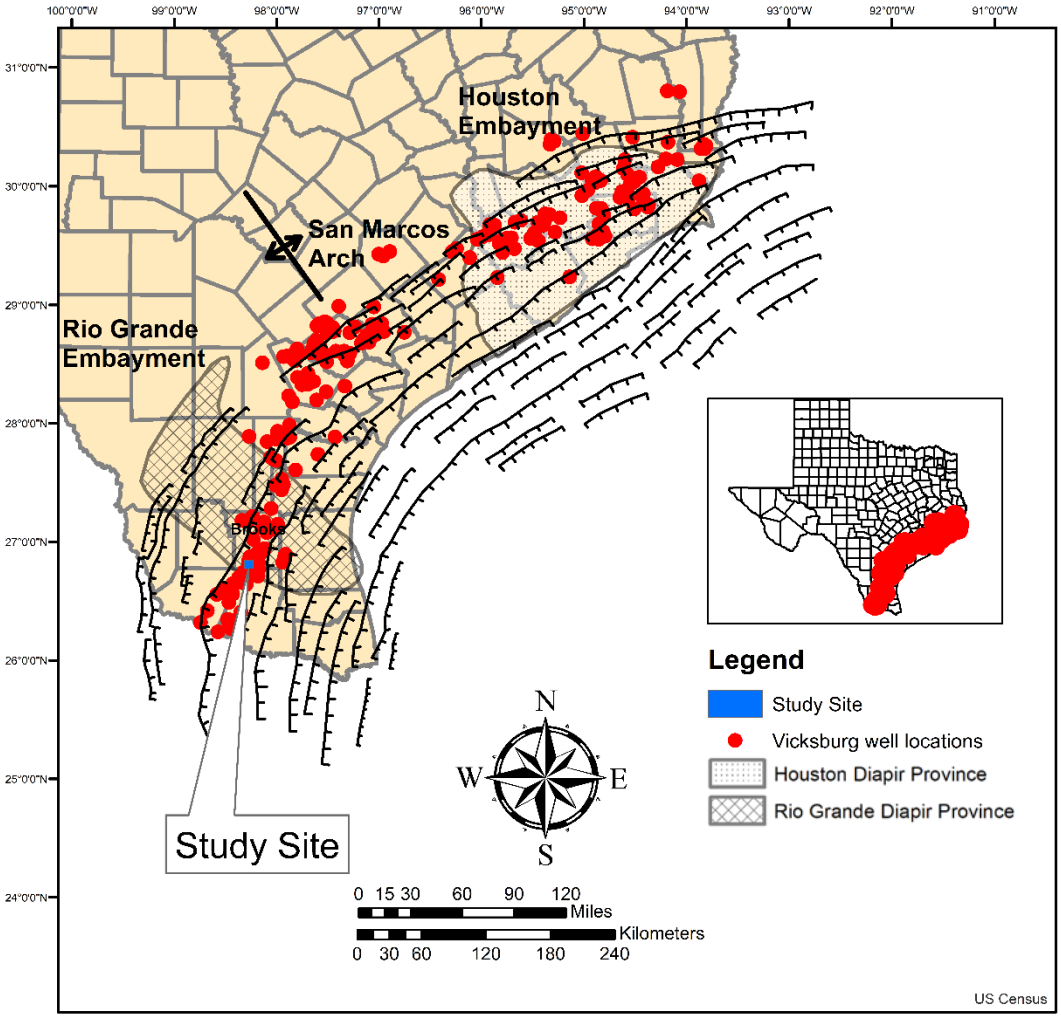

Figure 6: The VFZ with wells that have targeted the Vicksburg Formation.

sand and fault-shale assemblages (Zhou et al., 2019) in hydrocarbon accumulation and spatial distribution is of increasing importance to the success rates of hydrocarbon extraction.

The location of the study site within the RGE, specifically in Brooks County, has proven to be a prolifically productive oil and gas region. According to the Railroad Commission of Texas, gas production from January 2000 to January 2020 within Brooks County has exceeded 1 trillion cubic feet (TCF) and 17 million barrels of condensate (Railroad Commission of Texas, 2020). The informally named sand reservoir members of interest within the study site, V-102, V-17 and V-19, are three highly productive gas intervals. Interpretations of these three intervals in combination with the VX-Top, V-14, V-15, and V-16 will be the focus of this study. Specifically, secondary synthetic and antithetic faults will be explored to understand how they are affecting the accumulation quality within these reservoir intervals and how the secondary faults are affecting the spatial distribution of commercial producible quantities of hydrocarbons.

CHAPTER II

Data and Methodology

To investigate the effects of fault control on the LOVF reservoirs, a post-stack 3D seismic dataset was integrated with available well logging data (39 well logs; spontaneous potential [SP], gamma ray [GR], resistivity, and sonic) and three velocity surveys. Figure 9 shows a workflow of data and methods used in this study.

Seismic Data

A 3D seismic dataset for southern Brooks County, Texas, was donated to TAMU-CC by an oil and gas exploration company. The seismic survey consists of 289 in-lines, 279 crosslines, and 80,631 common depth points (CDP) that cover a 4.28-mile by 4.43-mile (6.88-kilometer by

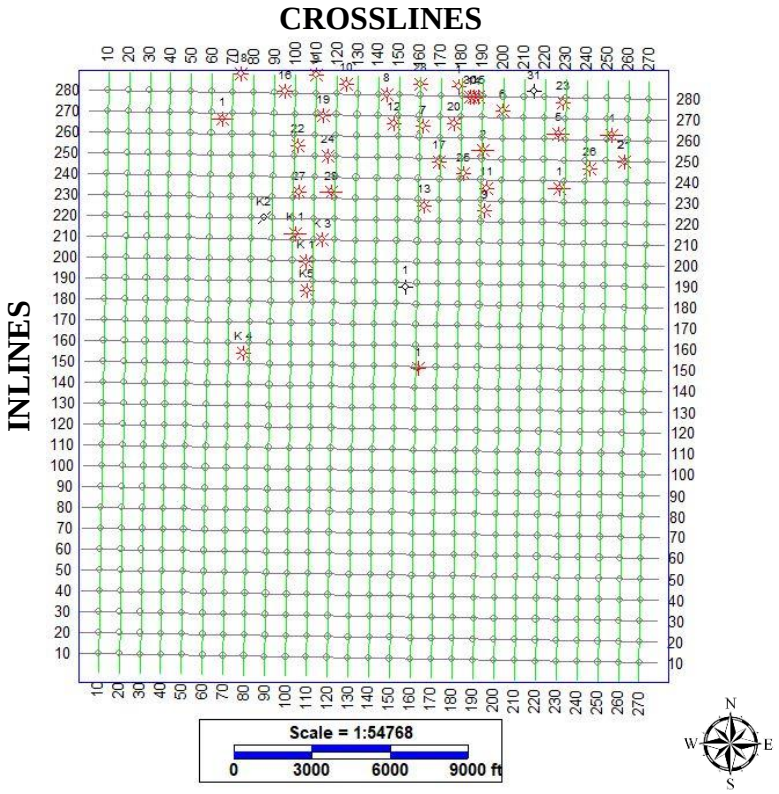

Figure 7: The 3D seismic grid used in this study displayed in the IHS Kingdom® software. The seismic grid contains 289 east-west in-lines and 279 north-south crosslines.

7.12-kilometer) grid (area: 49 km^2; Figure 7). The 3D seismic was a medium-effort proprietary survey acquired by the operator to guide development drilling. Acquisition parameters were industry standard for the 1995 survey. A post-stack migration was applied to the 3D seismic dataset. The seismic grid has a two-way travel time (TWT) recorded length of 3.5 seconds, with 80-foot (~ 24 m) CDP spacing, and a vertical sample rate of 4 seconds. IHS Kingdom® software has been utilized to read, process, and interpret the 3D seismic dataset.

Well Logs, Velocity Surveys, And Well Synthetics

Well logs serve as higher-resolution constraints for seismic data interpretation. The integration of well logs (lithologic and wireline logs) and seismic data allows both vertical and horizontal resolution to be optimized. A total of 39 wireline logs (SP, GR, resistivity, and sonic) were used in this study. Well logs have been used to pick informal unit tops in the upper, middle, and lower Vicksburg (VX-top, V-14, V-15, V-16, V-102, V-17, V-19). These picks were then loaded into IHS Kingdom® to improve picking of seismic horizons, to identify lithology, and to improve fault detection within the study area (Figure 9).

SP is generally used to define locations and boundaries of permeable beds (Asquith et al., 2004). In this study, SP logs were used to define the tops of the sand members (e.g., V-14, V-15, V-16, V-102, V-17, V-19) within the Vicksburg Formation.

GR logs were used to map sand and shale lithologic units by detecting radioactive particles within a given formation. Sandstones and carbonates tend to contain a lower concentration of radioactive elements (e.g., Thorium, Potassium, and Uranium) compared to shale (Asquith et al., 2004). In the case of the Vicksburg Formation, the sandstone reservoirs in the lower, middle, and upper sections were characterized by higher than expected gamma ray response. This is attributed

to the fact that these members are believed to contain high amount of volcanic sediments (Hosman, 1996) eroded from the upper Rio Grande Rift in New Mexico and deposited within the RGE. Hence, differentiating sand from shale members was conducted by integrating all available well logs (e.g., resistivity, sonic, SP, GR) (Figure 8).

Figure 8 shows a section of the Carter Ranch #7 well log with the study area. The gamma ray response within the sand reservoir intervals shows a high value of 50-65 API compared to the normal sand baseline (35-40 API). Examination of the SP, resistivity, and sonic responses also confirms the presence of sand packages within the V-17 and V-19 (Figure 8).

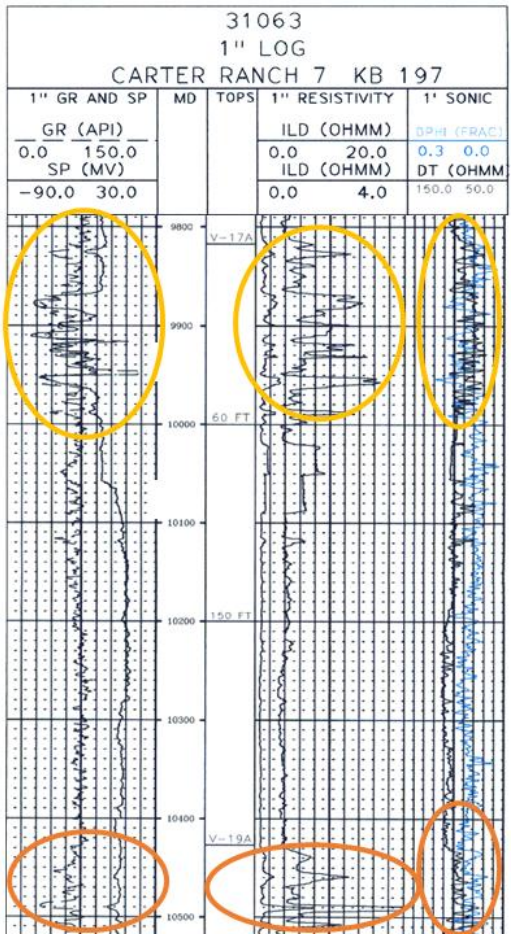

Figure 8: Carter Ranch #7 well log showing how the sand intervals (V-17 and V-19) look like. Sand intervals are outlined by colored circles.

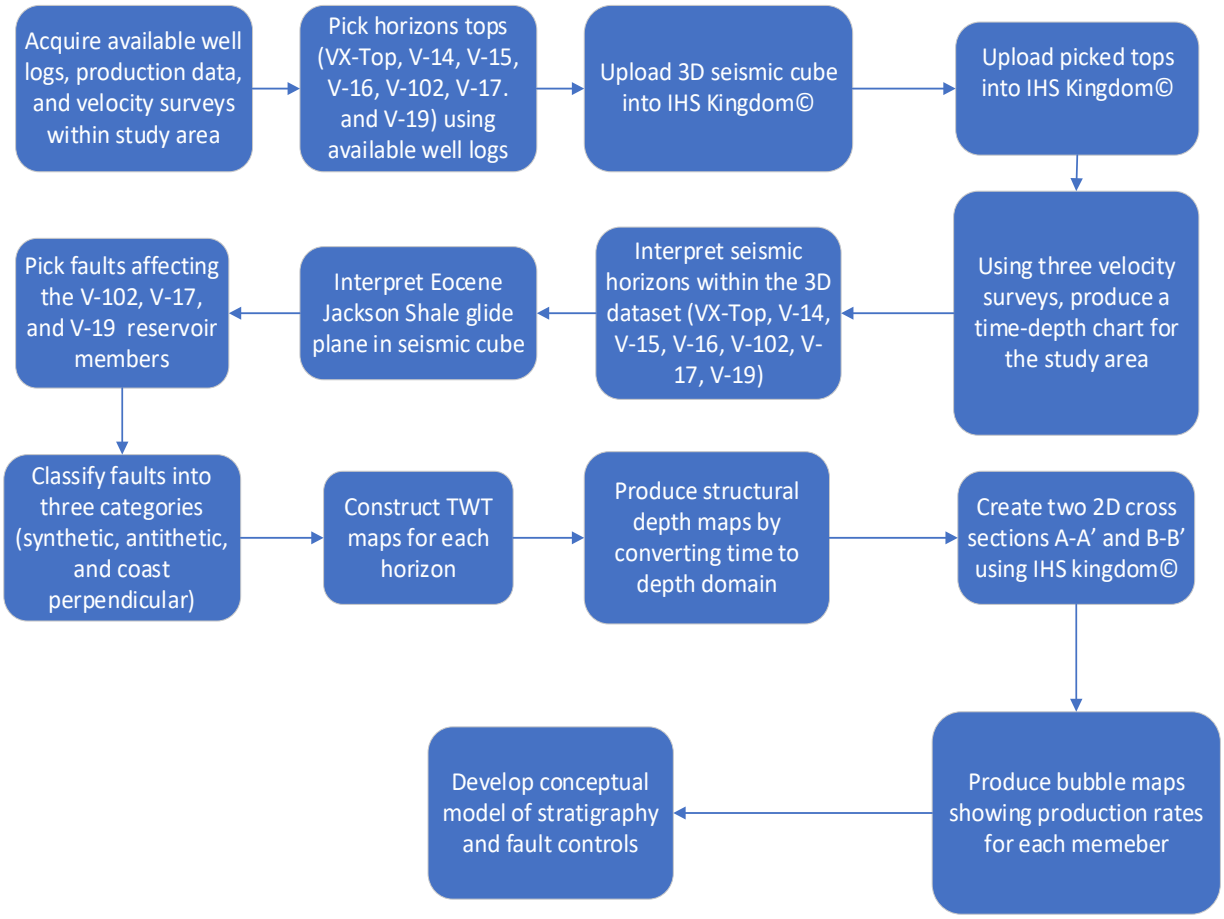

Figure 9: Workflow showing data and steps used in this study.

Three donated velocity check-shot surveys were used to model seismic data from the time domain to depth domain. The velocity check-shot locations are shown in Figure 10. Figure 11 shows the relationships between average velocity and TWT versus depth for the #1 ALA M Borglum, #1 Carter Ranch, and #1 GG Lopez wells. Inspection of Figure 11 indicates that the average velocity within the LOVF ranges from 9000 to 9800 ft/sec and there is a general increase in the average velocity with depth.

A single time-depth chart was generated for the study area by combining all three available checkshot surveys. A second order polynomial ($y= -2E-09x^2+0.0002x+0.0781$) was used to fit the

time-depth (T/D) relationship (Figure 11D). The generated time-depth chart has been applied to the entire 3D seismic survey.

To optimize the horizon interpretation process and parameters for the target reservoir members, a guiding well synthetic was generated from the (API 42047306690000, Energy Assets International Corp. #1 Carter Ranch) well and used to define the proper interpreted polarity of seismic horizons (e.g., peak, trough, inflection point). Well log synthetic seismograms were produced using IHS Kingdom® Synthetics software by integrating the average T/D, acoustic

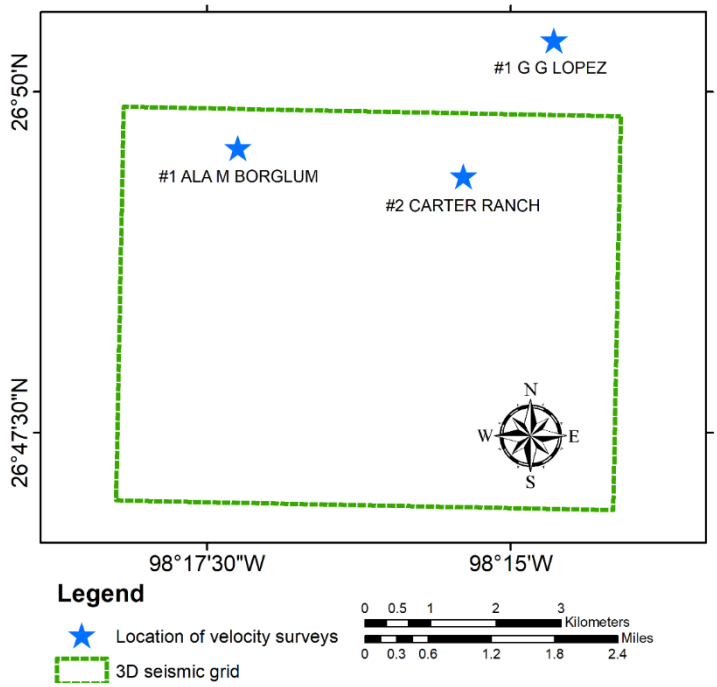

Figure 10: Locations of the velocity check-shot surveys. Also shown is the location of seismic grid.

impedance (AI), and reflection coefficient (RC) information (Figure 12). Inspection of Figure 12 indicates that VX-Top and V-102 reservoirs are corresponding to an interpreted inflection point (from positive to negative), while the V-14, V-15, V-16, V-17 and V-19 reservoirs are corresponding to interpreted peaks.

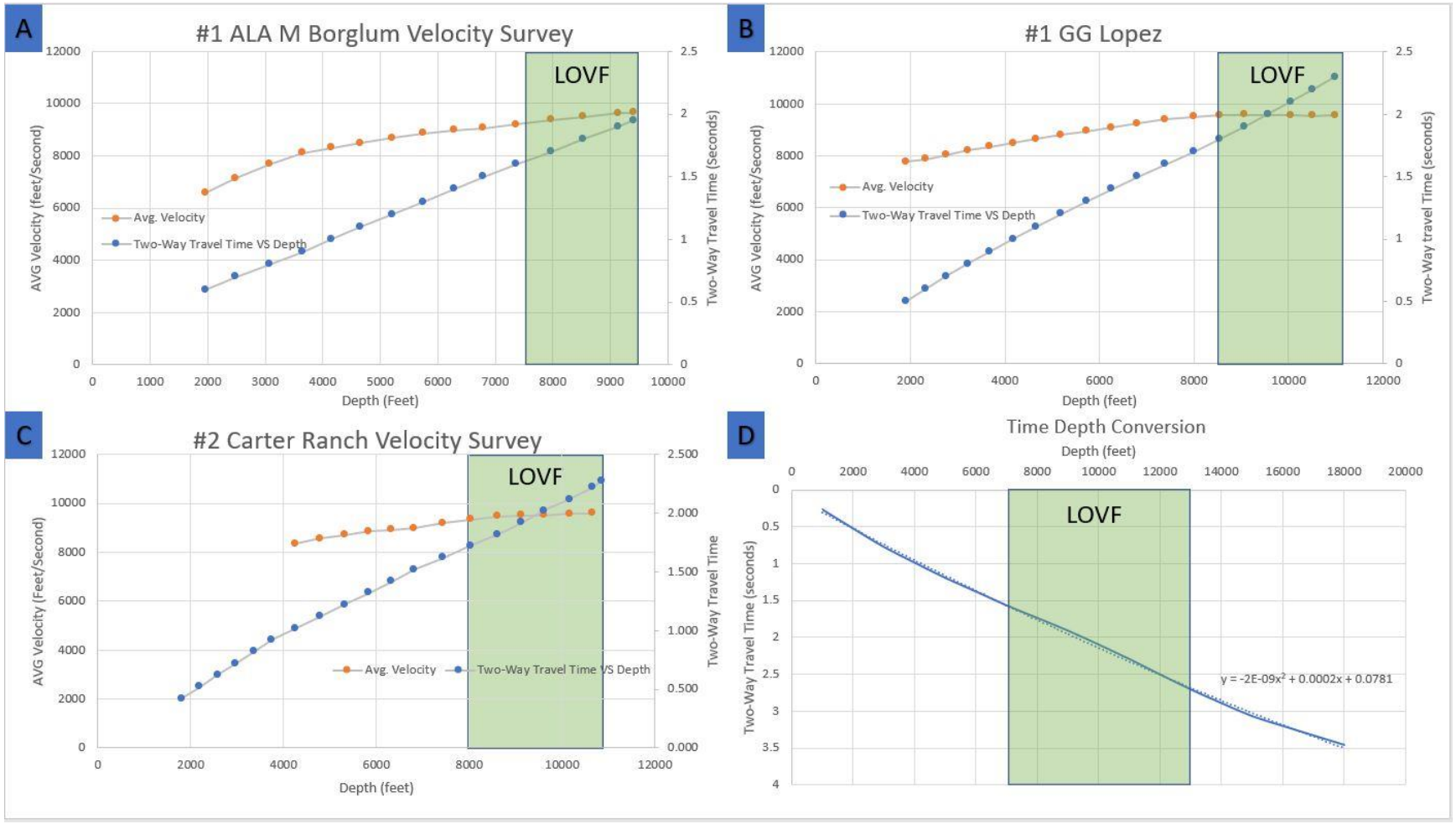

Figure 11: Average velocity (ft/sec) and TWT (sec) versus depth (ft) for the #1 ALA M Borglum, #1 GG Lopez, and #2 Carter Ranch wells.

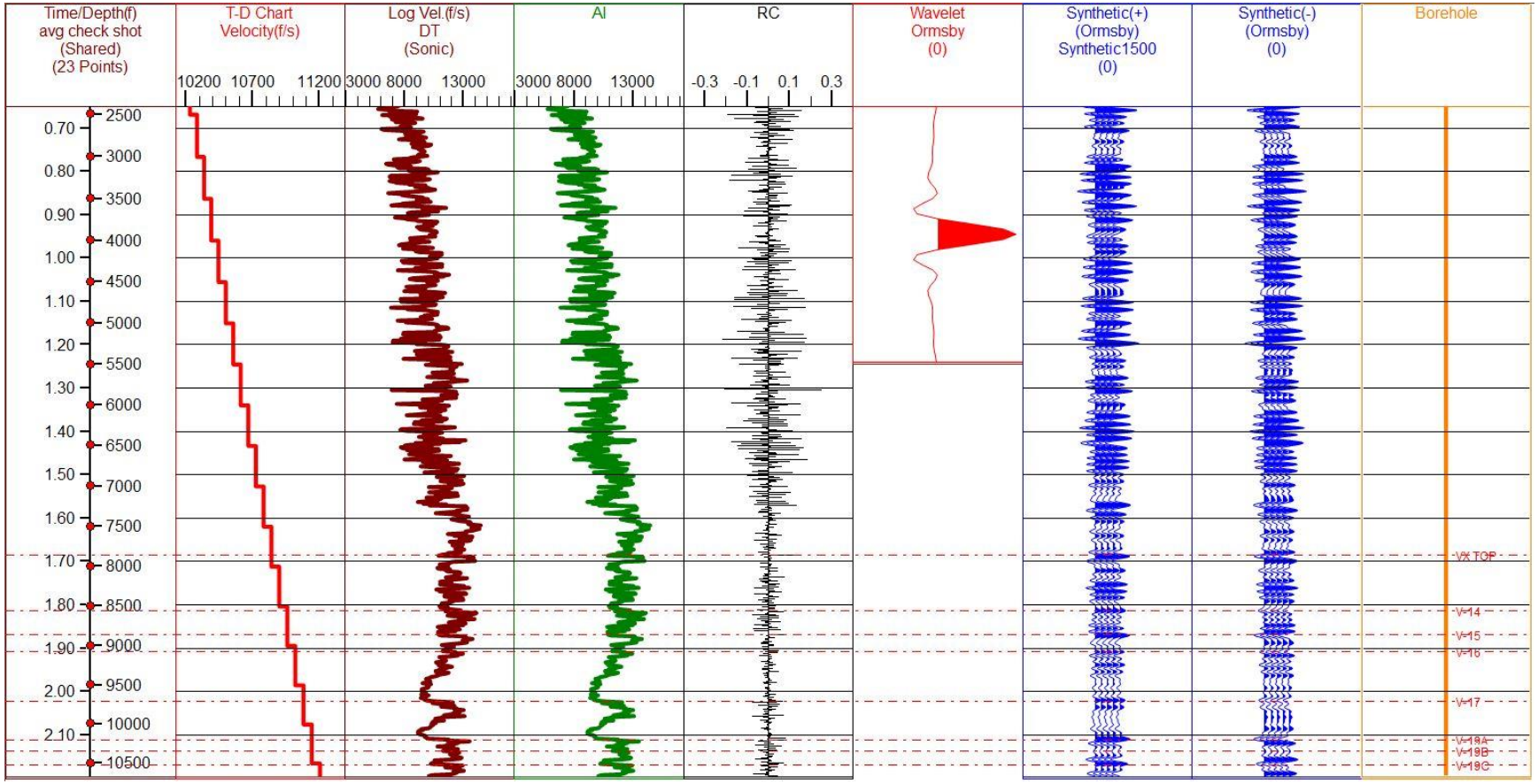

Figure 12: Well synthetic generated Acoustic impedance (AI) and reflection coefficient (RC) data for the Carter Ranch #3 well. Also shown are the VX-Top, V-14, V-15, V-16, V-17, and V-19 members.

Picking Interval Tops

Overall, the 3D seismic data utilized in this research has adequate quality, but the continuity of the seismic reflections varies extraordinarily vertically and horizontally from one reflection to another. Additionally, the seismic reflections vary within different seismic sections. Figure 13 shows an example of how the VX-Top, V-14, V-15, V-16, V-17, V-19 seismic reflections appear within the LOVF.

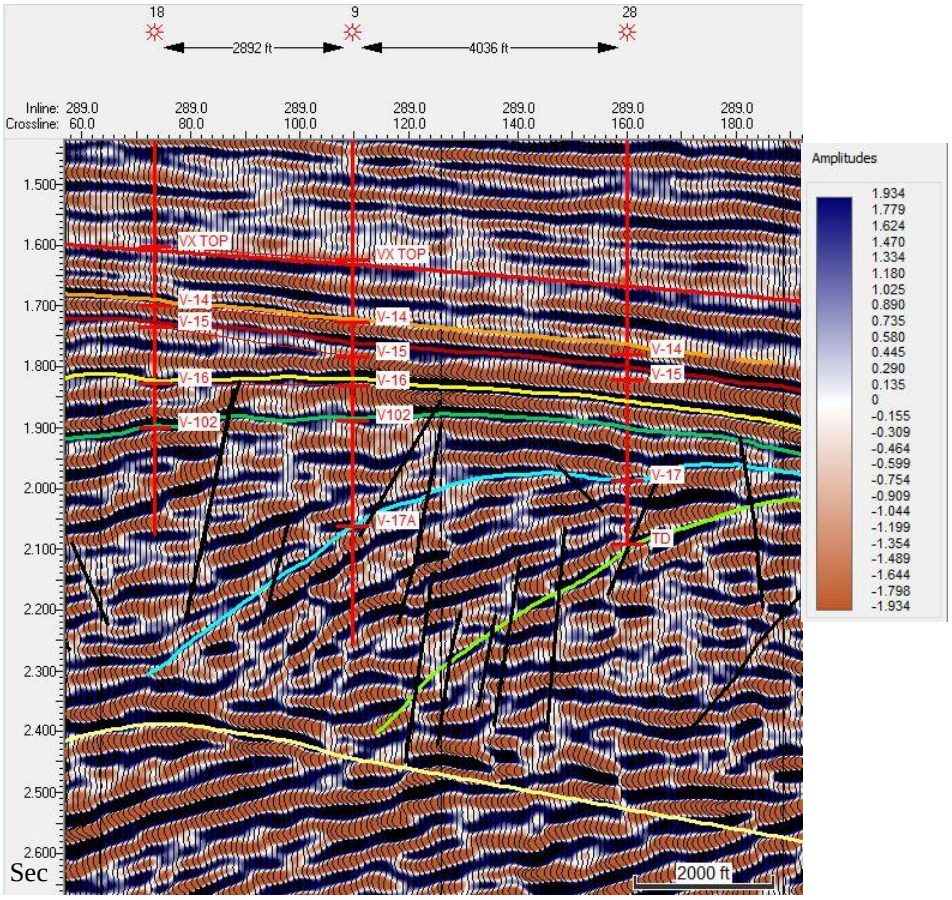

Figure 13: Seismic inline 289 showing the general quality of seismic reflections within the LOVF. Colored lines represent interpreted horizons (VX-Top, V-14, V-15, V-16, V102, V-17 and V-19).

IHS Kingdom® software picking tools have been utilized throughout the interpretation process to pick horizons and faults. “Automatic” 2D hunt picking tools were used to pick target horizons every 10 in-lines and 10 crosslines. Tops for target horizons were initially picked from

well logs. After initial “automatic” picking, target horizons on every in-line and crossline were picked and cross-checked using the “manual-linear fit” picking tool to optimize interpretation. Over 90,000 manual picks have been interpreted within this 3D seismic dataset as part of the research. Using 2D hunt picking tool in highly faulted horizons is not a proper option due to its inability to track horizons across highly faulted areas.

Picking seismic reflectors was initiated with the upper section of the Vicksburg Formation with the VX-Top horizon followed by the Eocene Jackson Shale decollement surface (glide plane). The reflectors corresponding to the V-14. V-15, V-16, V-102, V-17, and V-19 sands were then mapped. Mapping the upper-most horizon and the decollement surface created interpretation boundaries for the LOVF to be more precisely interpreted from the lower to the upper sections. Doing this enhanced understanding of the geologic structures within the LOVF. The upper section contains the VX-Top, V-14, and V-15, the middle section contains an unconformity and the V-16, and the lower section is comprised of the V-102, V-17 and V-19. The VX-Top is characterized by unclear seismic definition and discontinuity. This reflection has a moderate amplitude that makes it difficult to interpret. The V-14 is characterized by poor to moderate seismic definition but good

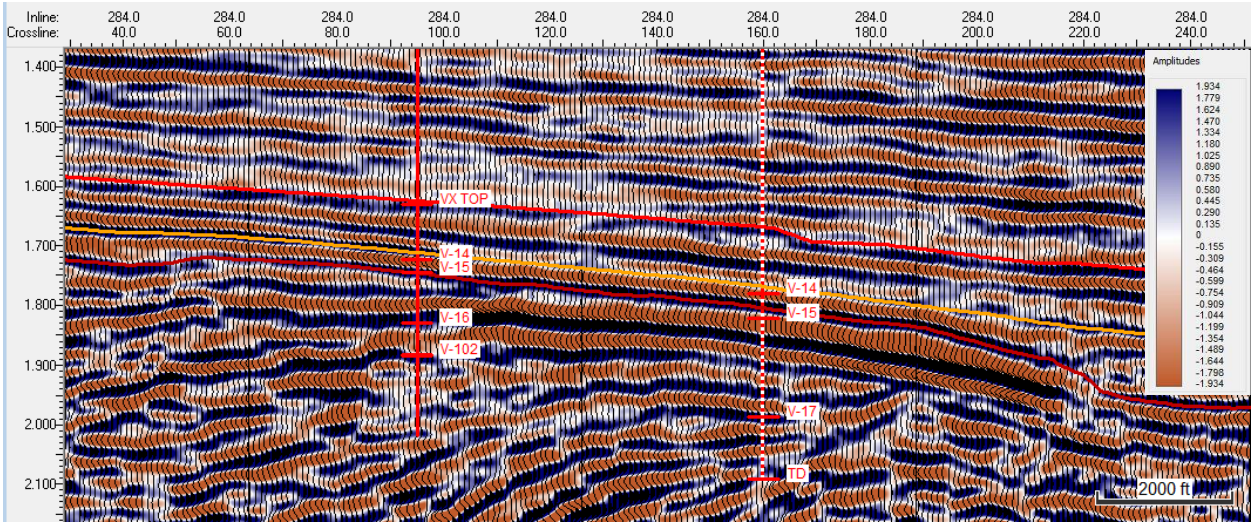

Figure 14: Seismic inline 284 showing the seismic horizons of the upper section of the LOVF.

spatial continuity. The reflection has a low to medium amplitude, which makes it straightforward to trace. The V-15 is characterized by good seismic definition and high spatial continuity; it has a high amplitude that makes it easy to trace across the survey area. Reflections of the VX-Top and V-14 are continuous while the V-15 seismic reflector diminishes east of the rollover anticline (Figure 14).

The unconformity is characterized by a negative amplitude or trough and high spatial coverage, making this seismic reflector a ready marker within the seismic sections. The V-16 is characterized by high seismic definition and high spatial continuity above the rollover anticline. East and west of the rollover anticline, the seismic reflection is moderate to poor. The reflection was expressed as a high frequency peak and high amplitude resulting in straightforward interpretation (Figure 15).

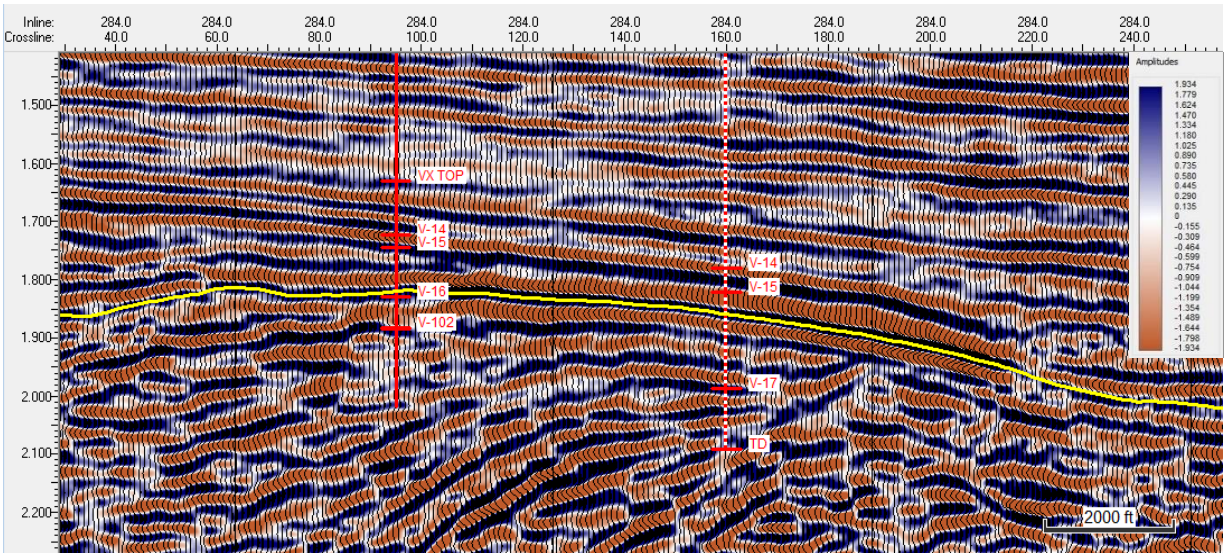

Figure 15: Seismic inline 284 displaying the seismic reflections of the middle section of the LOVF.

The V-102 reflector is characterized by a moderate to poor seismic definition with low spatial continuity. The reflection has a low amplitude making this reflector difficult to interpret. The V-17 and V-19 are characterized by good seismic definition and low spatial continuity. The

reflections have a medium to high frequency peak and a high amplitude; although the definition of the seismic reflector is good, the continuity is poor. This is due to the highly faulted interval making the reflection gradually weaker to the east and west of the rollover anticline (Figure 16).

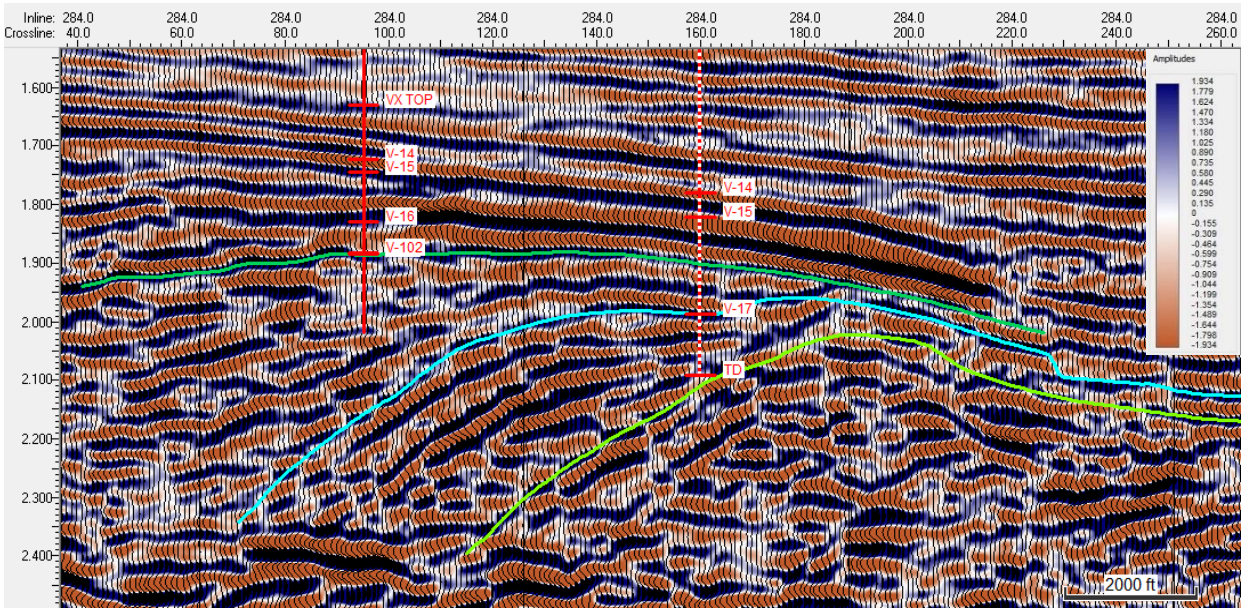

Figure 16: Displaying the seismic reflection of the lower section of the LOVF. Seismic reflections are discontinuous to the east of the rollover anticline.

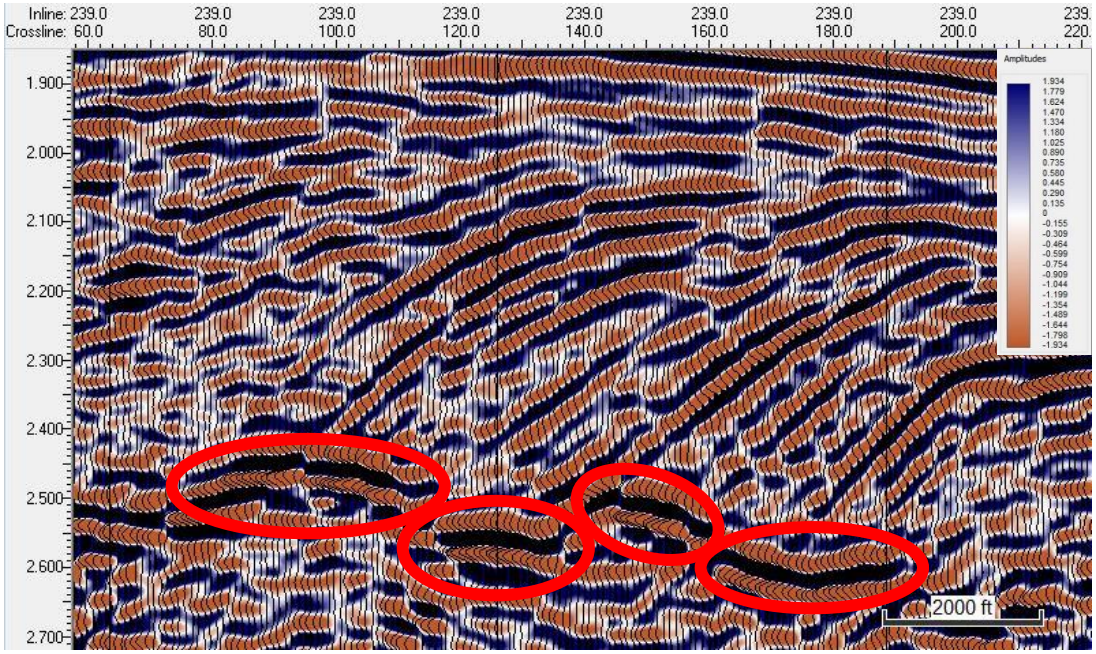

Figure 17: Downlapping onto the Eocene Jackson Shale glide plane seismic packages, indicated by red circles.

Interpreting the Eocene Jackson Shale glide plane is essential to investigating the structure produced by the VFZ. No wells within the study area penetrate the Eocene Jackson Shale; therefore, the seismic expression of the decollement was relied upon to interpret and map the Eocene glide plane. The downlap of wedges on the glide plane are marked by red circles in Figure 17 and were interpreted to be the Eocene Jackson Shale fault-bound contact.

Mapping Faults

As a part of the comprehensive analysis, faults were interpreted and mapped within the 3D seismic dataset using IHS Kingdom® software. Picking faults affecting the reservoir intervals is an essential step to determining fault control. The fault picking tool was used to digitize fault planes and to determine their continuity. Interpreting faults interactively while interpreting horizons is crucial to fully comprehending the structural development of the rollover anticline and how secondary faults are affecting the interval.

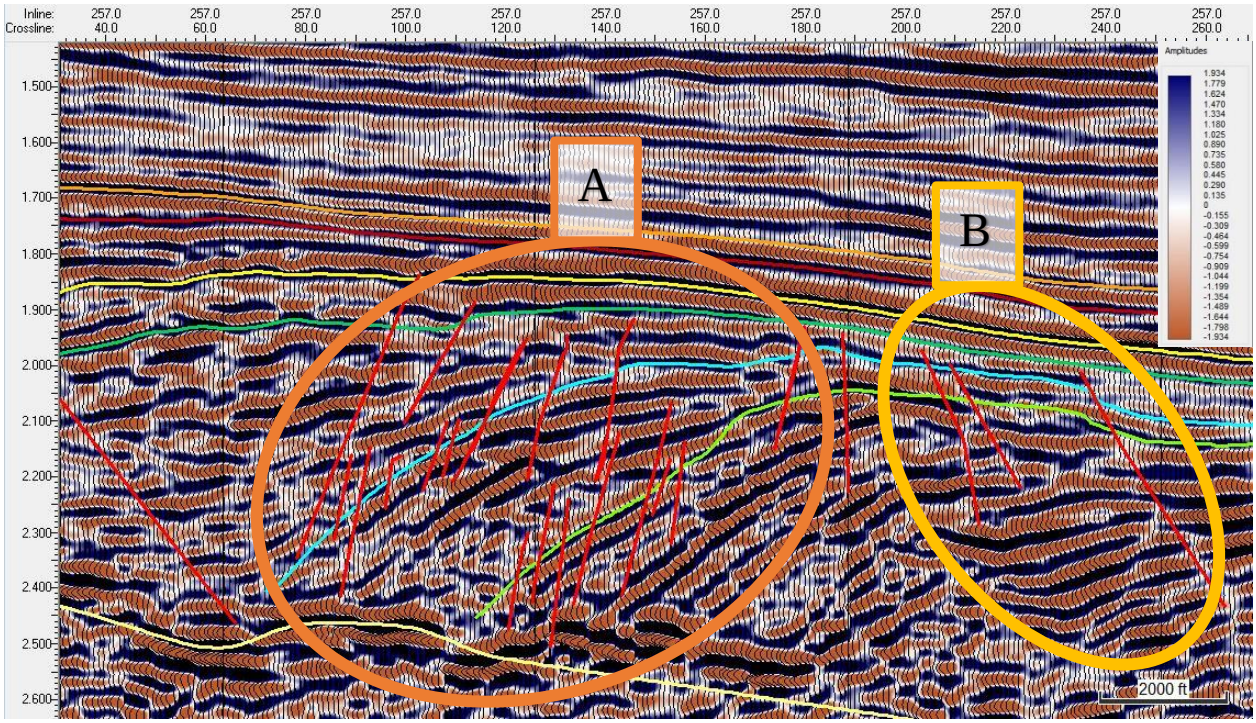

Figure 18: Seismic inline 257 displaying fault clusters A and B.

Three clusters of secondary faults affecting the Vicksburg Formation were interpreted within the study area: antithetic faults (those dipping west, cluster A), synthetic (those dipping east, cluster B) (Figure 18), and coast-perpendicular faults (dipping to the south and north, cluster C) (Figure 19). All faults within these clusters are extensional or “normal” gravity-driven faults. Picking faults was characterized upon displacement of horizons on the down-thrown block. Consistently interpreting how the faults are displacing the interval is crucial to accurately interpreting how the interval is being affected by the secondary faults and how the rollover anticline structure is being affected by the VFZ. Major faults affecting horizons were mapped to further infer fault control on migration, accumulation, and segmentation.

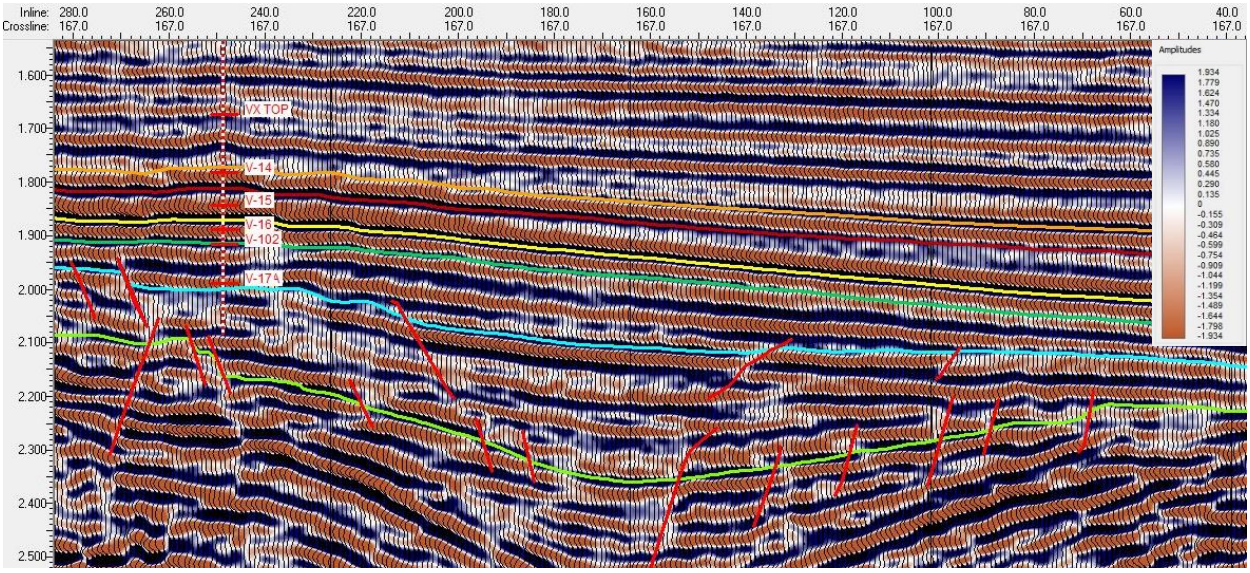

Figure 19: Seismic crossline 167 displaying fault cluster C.

CHAPTER III

Results

Well Correlation

Two well-log cross sections were constructed to examine the general attitude of the LOVF within the study area. Well logs were correlated along two cross sections located within the northern section of the seismic grid (Figure 20). The A-A' coast perpendicular cross section was constructed to validate the rollover anticline structure produced by the VFZ, whereas the B-B' coast parallel cross section was generated to explain structural variations within the study area.

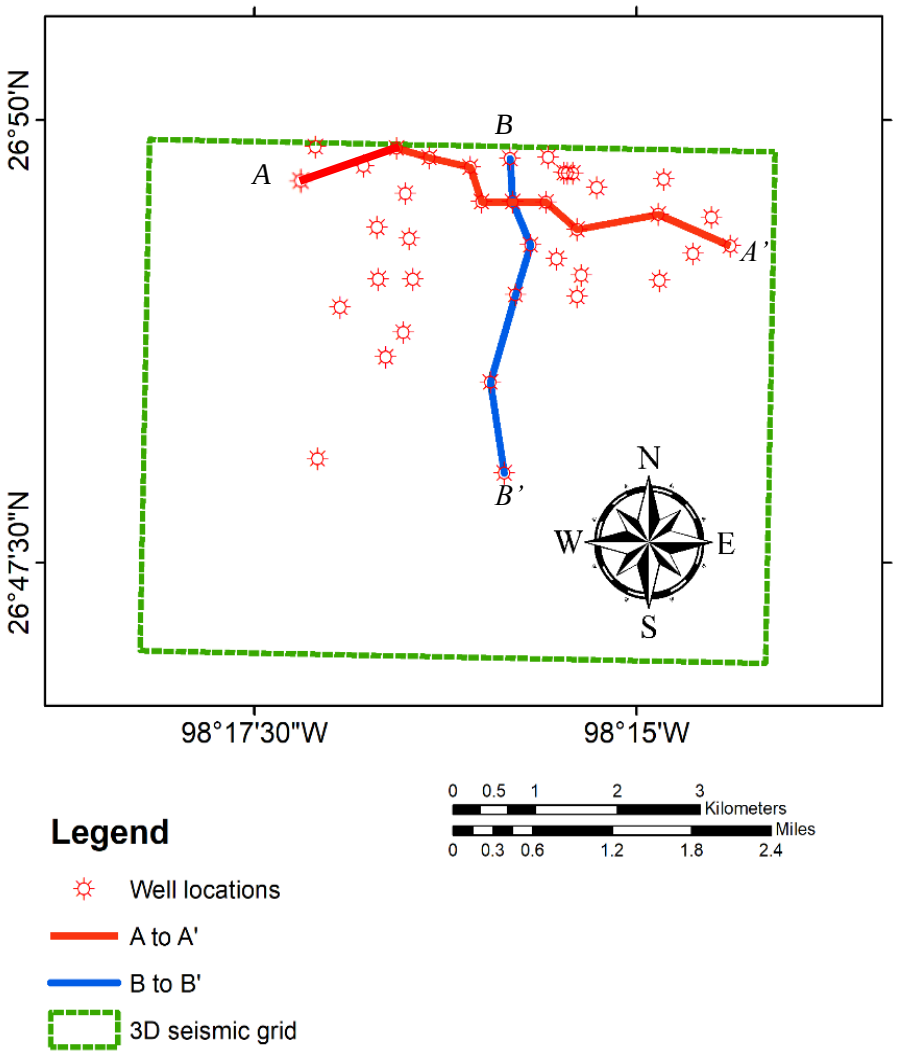

Figure 20: Well and cross section locations (A-A' and B-B').

Cross section A-A’ (Figure 21) shows the VX-TOP, V-14, and V-15 gradually dipping eastward towards the coastline. Counter to this, west dipping V-16, V-102, V-17, and V-19 are being affected by the listric fault developing the rollover anticline. The Coastal Pettus #1 well is the closest well to the listric fault, showing the VX-top, V-14, V-15, and the V-102 with the V-17 and V-19 horizons grounding out against the low side of the decollement before reaching this well. The Carter Ranch #4 well is the eastern most well to show the V-17 before the V-17 dips away from the coast towards the listric fault and glide plane. Carter Ranch #7 is one of the most important wells because it is the western-most well to show how the V-17 and V-19 before the V-19 dips towards the glide plane.

The location of cross section B-B’ (Figure 20), was chosen to illustrate structural variations through the rollover anticline into the southern portion of the seismic dataset striking north-south, perpendicular to the coastline. Cross section B-B’, includes five wells, from north to south (Figure 22): Jones Borlgum #1, La Rucias #7, La Rucias #17, La Rucias #13, and Jones AC #1 wells. The Jones-Borglum #1 was the discovery well for this field and well is the most northern well displaying the VX-Top, V-14, and V-15. Key horizons are gradually dipping south to the Jones AC #1 well (most southern well in cross section B-B’), showing little to no impact from the major listric fault. The V-16, V-102. V-17, and V-19 do not show a gradual dip but rather a rapid plunge away from the rollover anticline into the syncline of the middle section of the seismic grid. The V-17 horizon is plunging over 900 feet through the cross section.

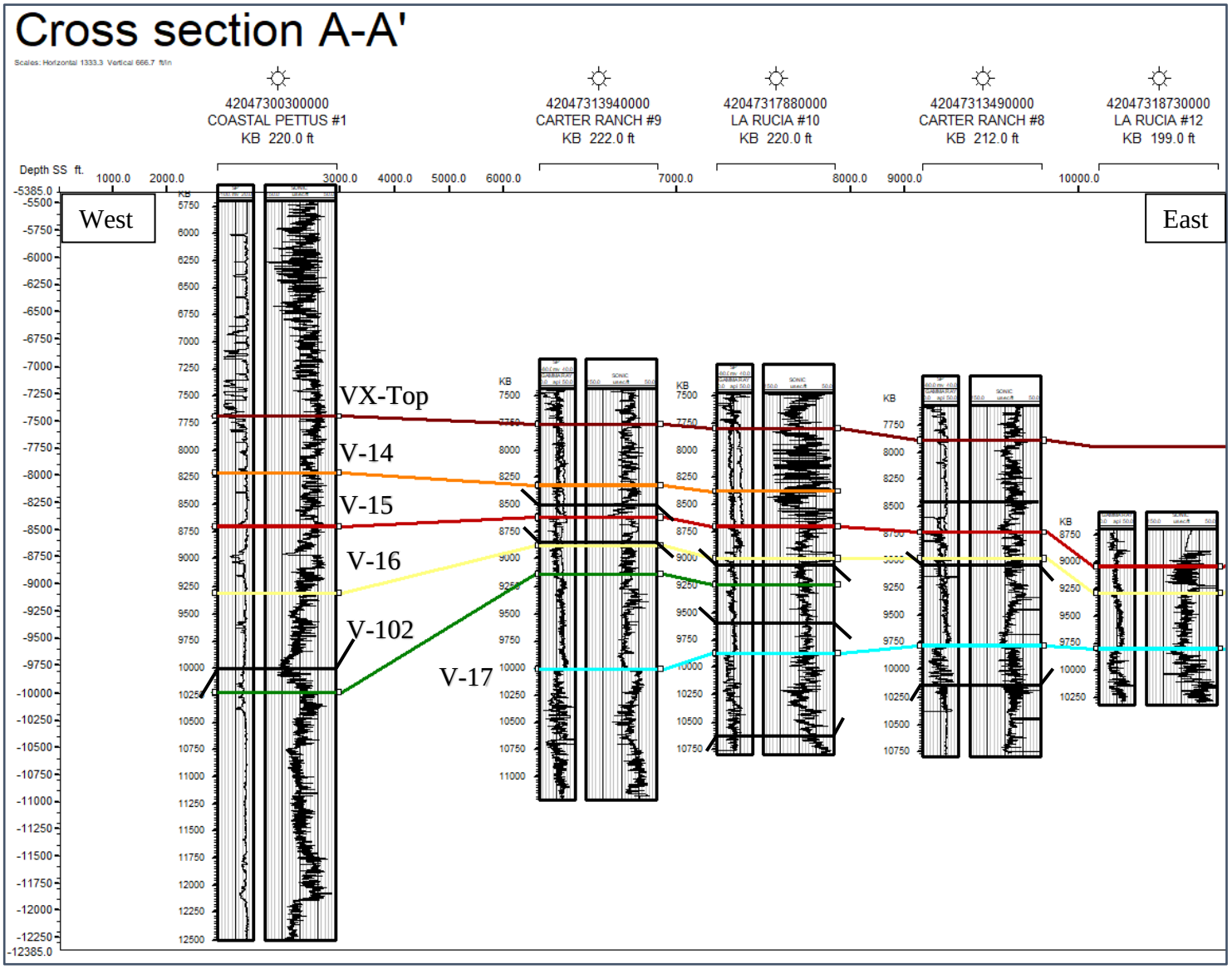

Figure 21: Cross section A-A' showing VX-TOP (brown), V-14 (orange), V-15 (maroon), V-16 (yellow), V-102 (dark green), V-17 (light blue), V-19 (light green).Continued on next page.

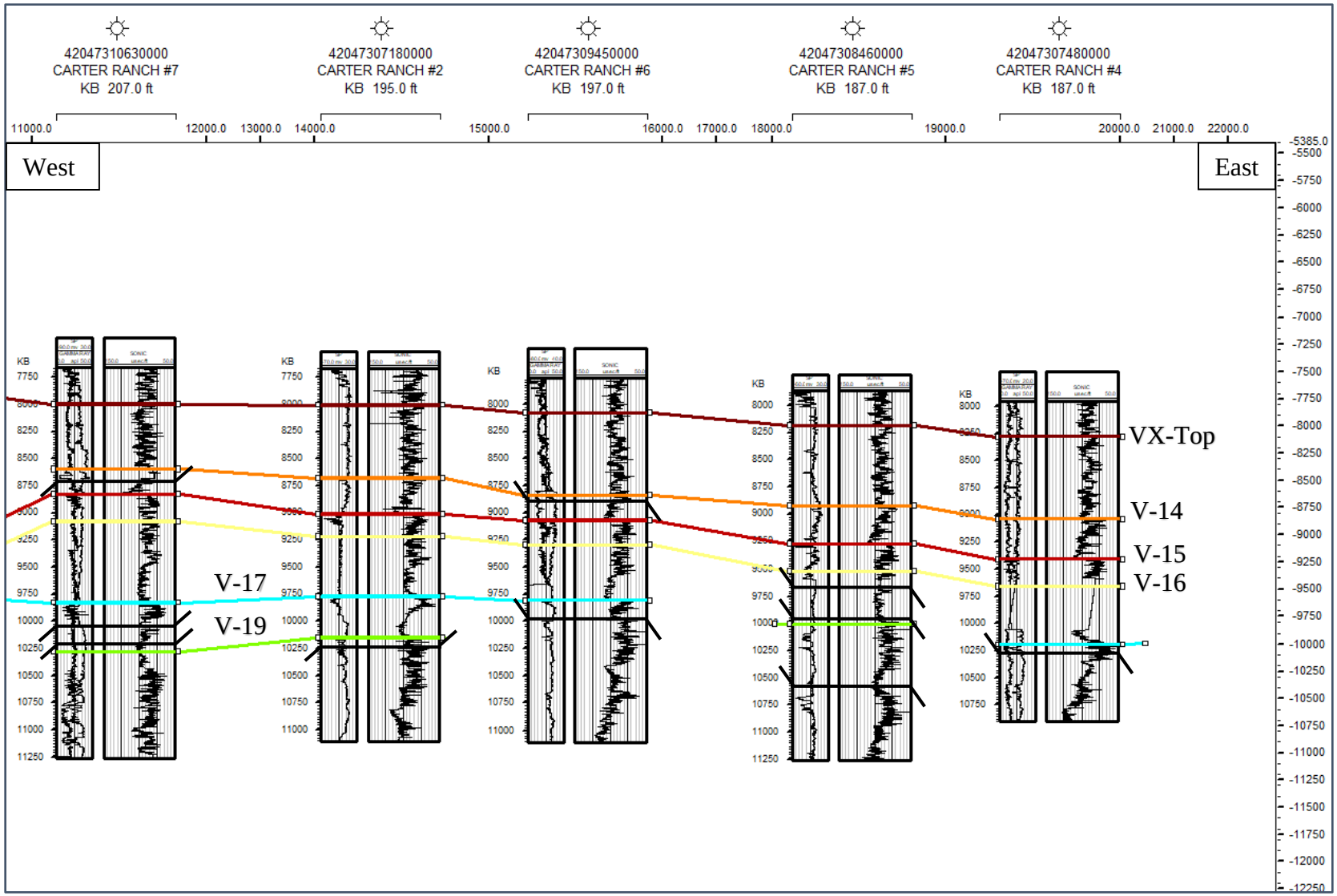
42047310630000
CARTER RANCH #7
KB 207.0 ft
42047307180000
CARTER RANCH #2
KB 195.0 ft
42047309450000
CARTER RANCH #6
KB 197.0 ft
42047308460000
CARTER RANCH #5
KB 187.0 ft
42047307480000
CARTER RANCH #4
KB 187.0 ft
West
East
VX-Top
V-14
V-15
V-16
V-17
V-19

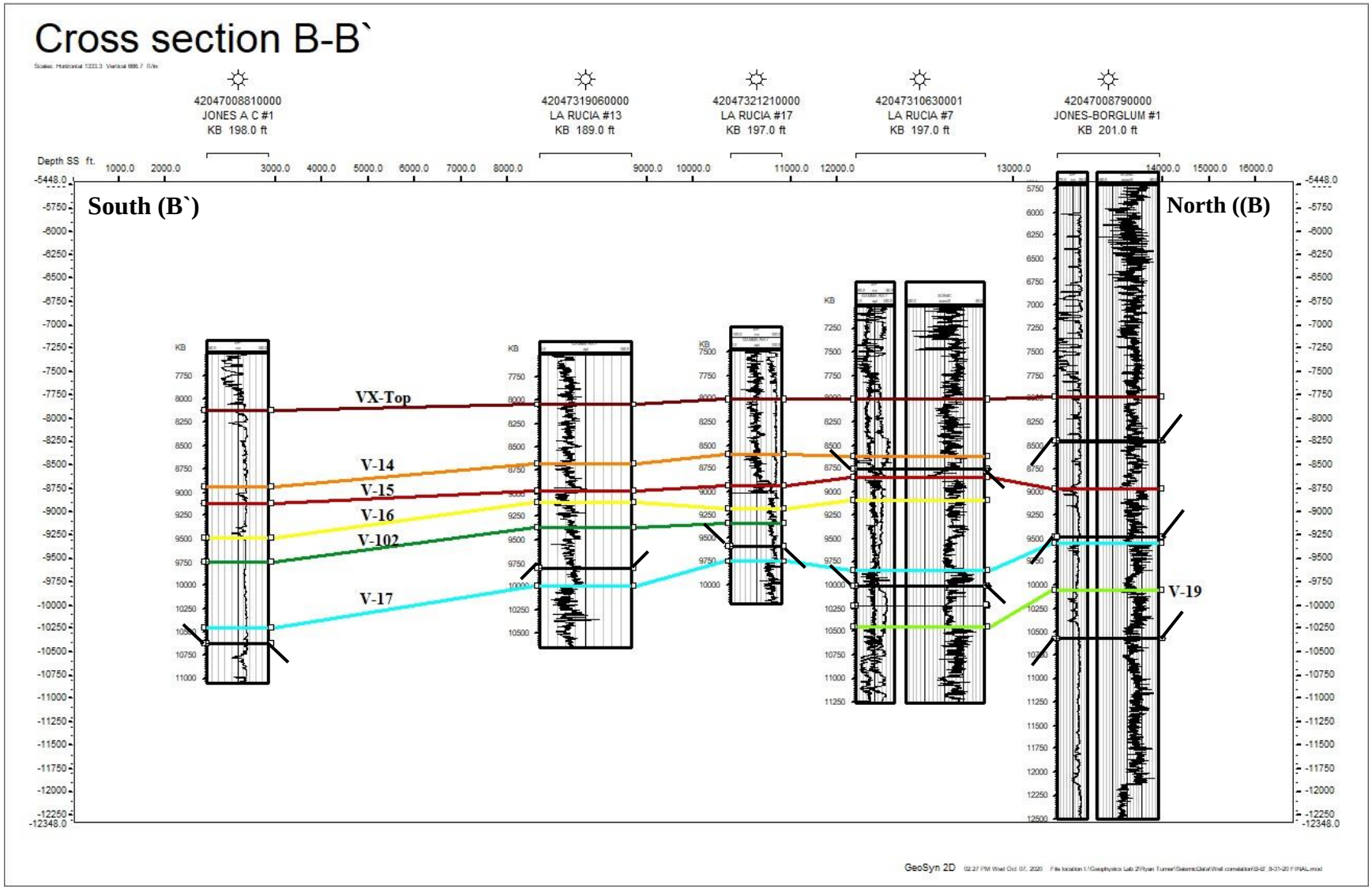

Figure 22:Cross section B-B showing VX-TOP (brown), V-14 (orange), V-15 (maroon), V-16 (yellow), V-102 (dark green), V-17 (light blue), V-19 (light green).

Eocene Jackson Shale Glide Plane

The geometry of the upper, middle, and lower Vicksburg Formation is principally controlled by the Vicksburg Fault Zone and the Eocene glide plane. Mapping the Eocene glide plane is based upon the high amplitude reflection bounded by low amplitude reflections (Figure 23). The amplitude change is caused by a shift in lithology from prograding deltaic deposits to shelf edge marine shale deposits. Dilation of the V-17 and the V-19 sand-prone reservoir packages on the downthrown block of the VFZ, above the Jackson, is creating a distinctive velocity pullup (Figure 23). This feature is primarily caused by a sudden change from high-velocity sands to slower-velocity shales below. The sound wave is traveling at a higher velocity through the V-17 and V-19 sand reservoirs and then it abruptly decreases velocity in the underlying thick marine Jackson shale.

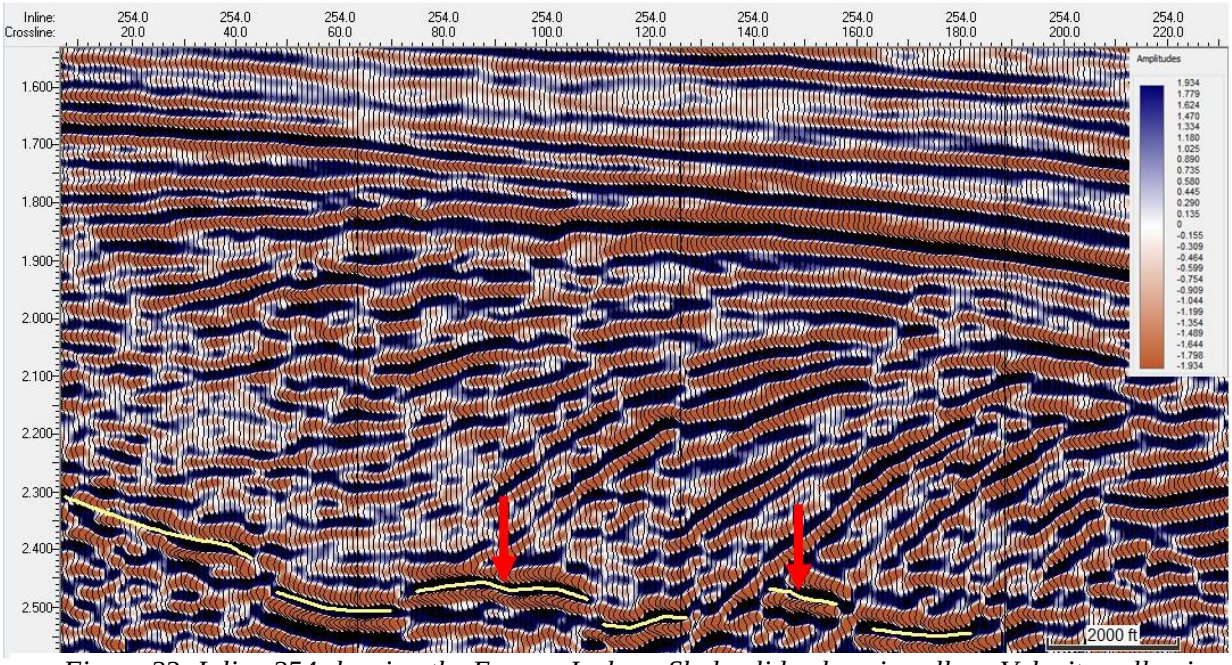

Figure 23: Inline 254 showing the Eocene Jackson Shale glide plane in yellow. Velocity pullup is indicated by red arrows

The velocity pullup is causing undulation within the glide plane, as expected on time domain data. This artifact could be taken care of by using a depth migration seismic section. Listric normal fault glide plans rarely dip more than 3 degrees; therefore, the glide plane was interpreted

to be a shallow dipping surface striking north-east, south-west, and consistently dipping toward the Gulf of Mexico (GOM) (Figure 23).

The Two-way Travel Time (TWT) map of the Eocene glide plane (Figure 24) shows the glide plane striking north-east and south-west, dipping towards the Gulf. The velocity expansion is located where the V-17 and V-19 intervals ground out onto the decollement surface.

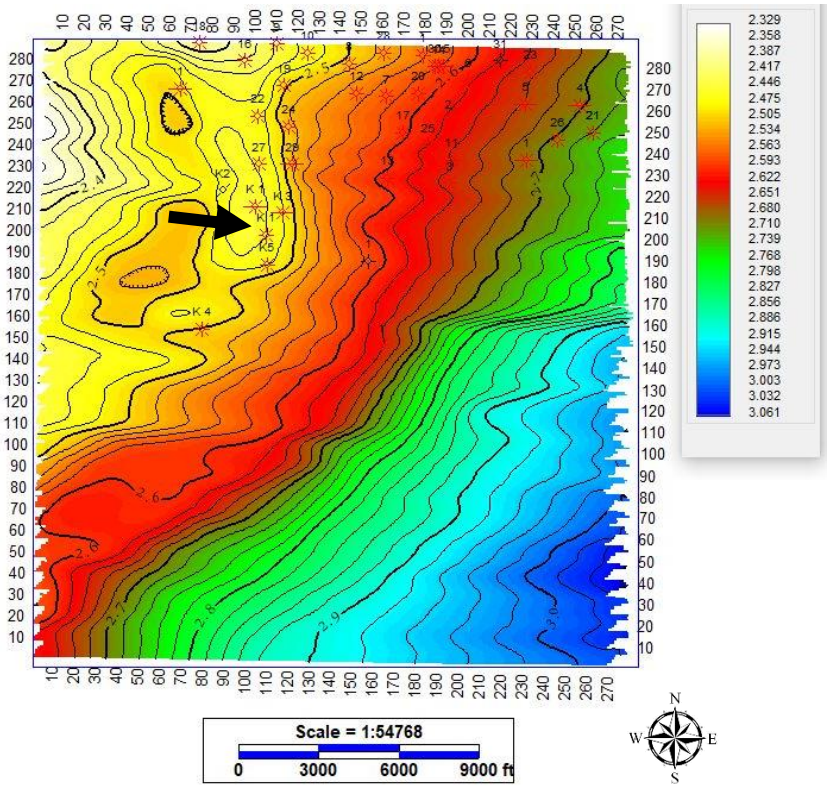

Figure 24: TWT map of the Eocene glide plane (time in seconds). Black arrow indicates area of velocity expansion.

Upper Vicksburg Section

The upper section of the LOFV is not affected by the VFZ, resulting in consistent east dip. Seismic horizons within this section (e.g., VX-Top, V-14, and V-15) are likewise less affected by secondary faults, although in the northeastern section of the study area (Figure 25, Figure 26, and

Figure 27) the TWT maps indicate a few coast-perpendicular faults affecting these intervals. The origin of these coast-perpendicular faults will be discussed later in this chapter.

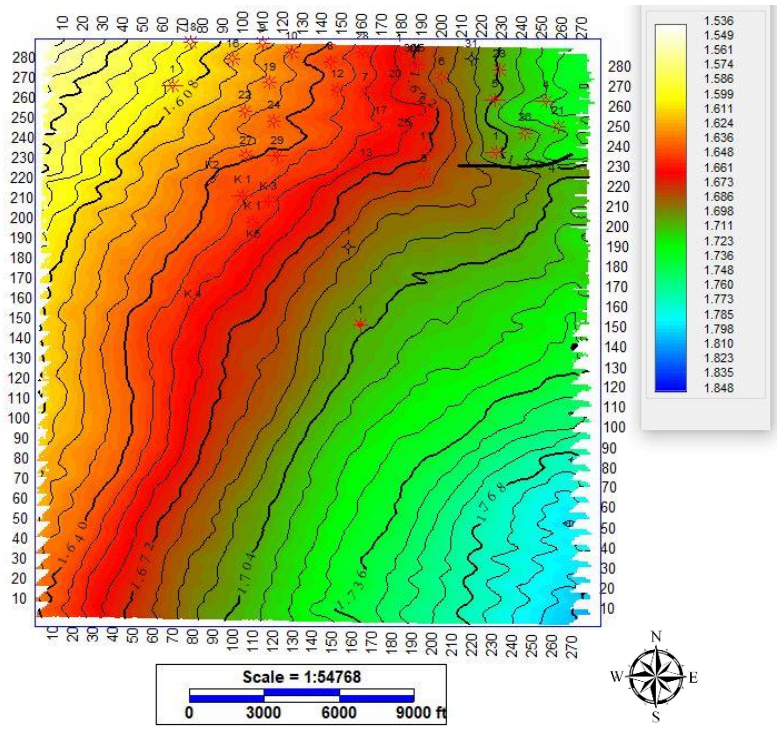

Figure 25: TWT map of the VX-Top horizon (time in seconds) with one major coast perpendicular fault in the northeastern section of the map.

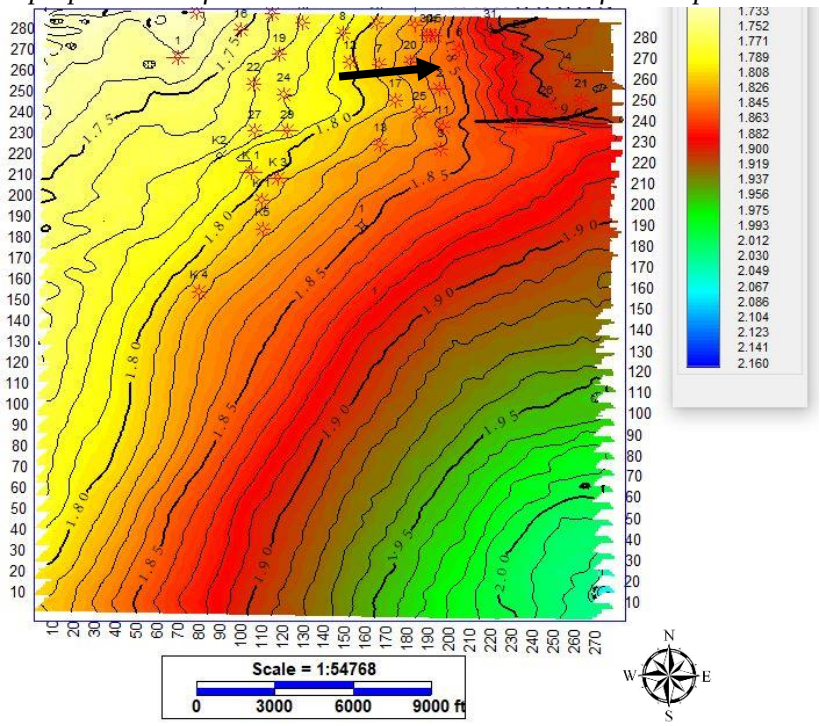

Figure 26: TWT map of the V-15 horizon (time in seconds). A graben is indicated by a black arrow.

The VX-Top, V-14, and V-15 TWT maps (Figure 25, Figure 26, and Figure 27) show the northeast-southwest strike of these horizons with a gradual dip towards the Gulf. Two coast-perpendicular faults are affecting these horizons and developing a graben in the north-eastern section of the study areas as indicated by examination of the TWT map (Figure 27).

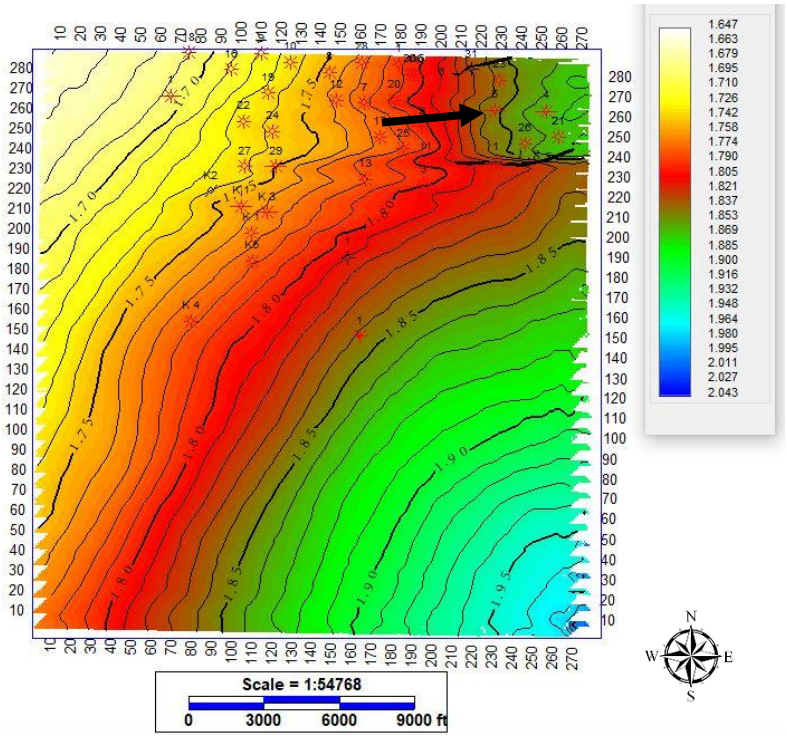

Figure 27: TWT map of the V-14 horizon (time in seconds). A graben is indicated by a black arrow.

Middle Vicksburg Section

The middle Vicksburg section of the LOVF is distinguished by an unconformity and contains the V-16 interval (Figure 4). The unconformity is caused by a transgressive systems tract, a transition from the low stand systems tract seen in the lower section of the Vicksburg. The V-16 TWT map (Figure 28) shows a northeast-southwest strike with a gradual dip towards the Gulf and secondary faults affecting the interval. A few secondary coast-parallel and coast-perpendicular faults were outlined in seismic sections and the TWT map indicating the interval is less affected by the VFZ.

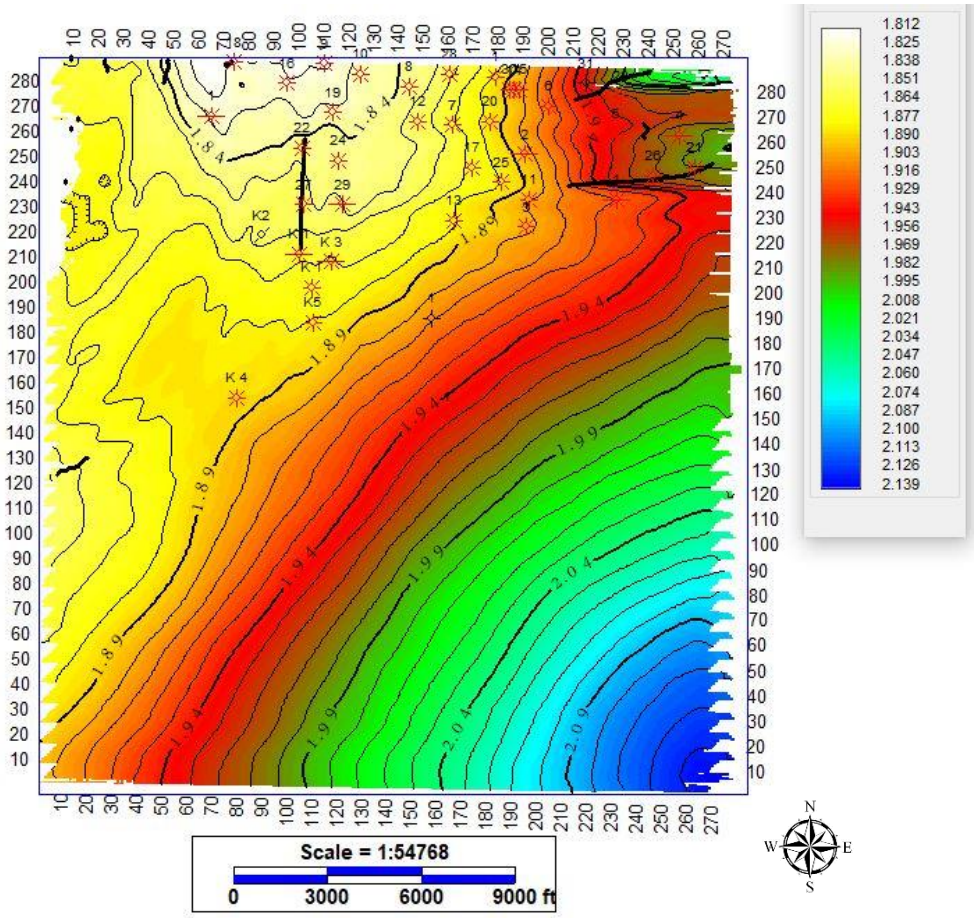

Figure 28: TWT map of the V-16 horizon (time in seconds)

Lower Vicksburg Section

The lower Vicksburg section is highly influenced by the VFZ, producing a rollover anticline. The mapped V-102, V-17, and V-19 intervals comprise the lower section. Because of the syndepositional relationship, these reservoir intervals are highly affected by secondary faults developed from the rollover anticline structure. Three types of faults are affecting the reservoir intervals, antithetic (cluster A, Figure 29), synthetic (cluster B, Figure 29), and coast-perpendicular faults (cluster C, Figure 30). The fault geometry within the rollover anticline is suspected to control accumulation and migration of hydrocarbons, and based upon the reservoir being investigated, the spatial distribution varies from the V-102 (Figure 31), V-17 (Figure 32), and the V-19 (Figure 33)

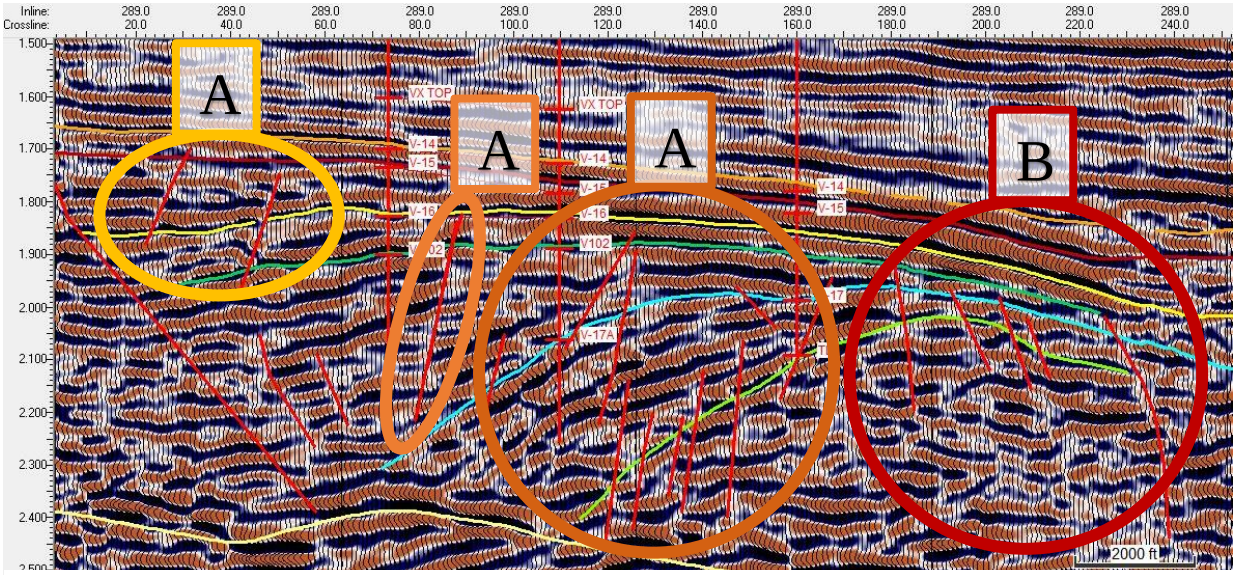

Figure 29: Seismic inline 289, colored circles indicate fault clusters affecting the V-102, V-17 and V-19.

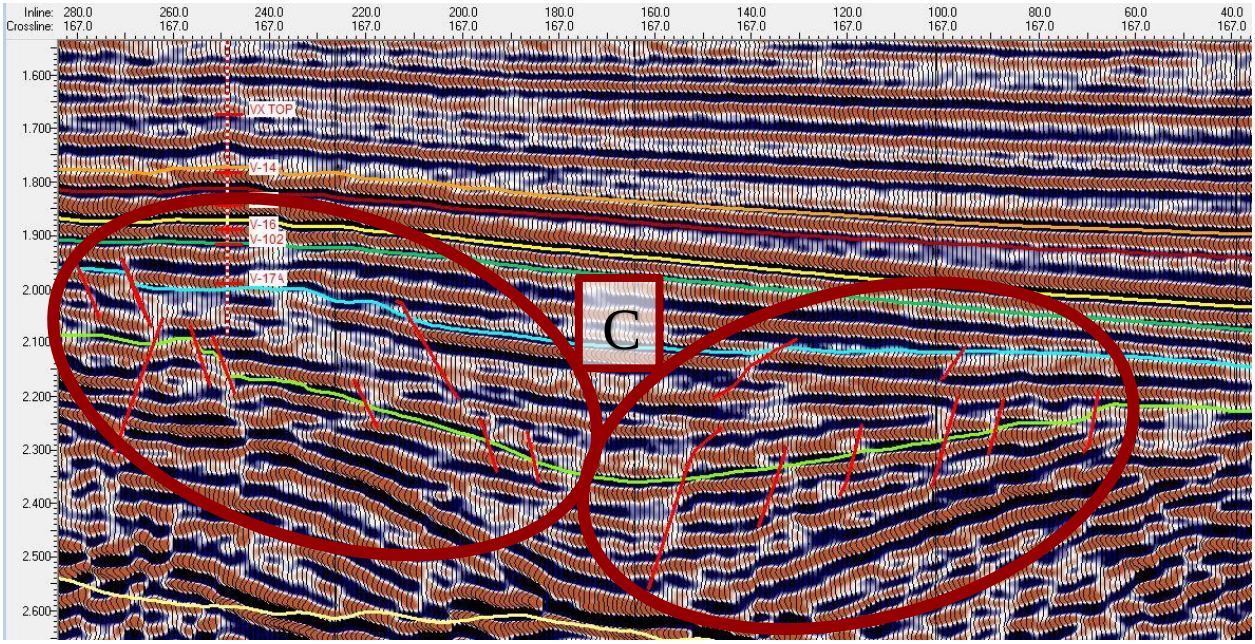

Figure 30: Seismic crossline 167, colored circles illustrate cluster C faults.

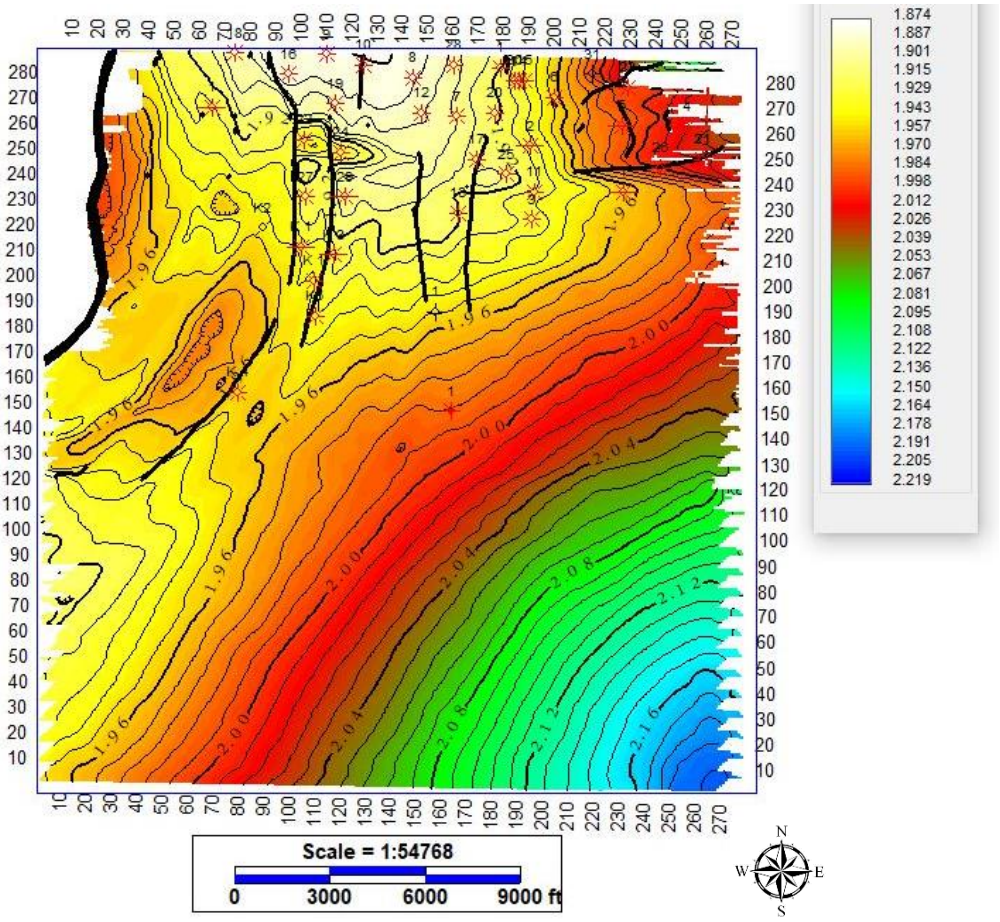

Figure 31: TWT map of the V-102 interval (time in seconds)

The TWT map of the V-102 interval illustrates how the VFZ, cluster A, and cluster B faults are affecting the interval (Figure 31). The TWT map indicates the V-102 interval is striking north-east and south-west. The section of the V-102 at the highest point on the rollover anticline is dipping towards the VFZ in the north-eastern corner of the grid, while the eastern section of the V-102 is dipping towards the Gulf. Fault concentration within the interval indicates cluster A faults are affecting the dip, accumulation, and spatial distribution within the V-102 sand reservoir (Figure

29).The TWT map of the V-17 interval (Figure 32) suggests increasing fault concentration with increased depth within the LOVF. Fault clusters A, B, and C have increased from the V-102 to the V-17, indicating the V-17 is highly affected by the VFZ (Figure 29 and Figure 30). Fault clusters A and B trend with the VFZ, while fault cluster C trends perpendicular to the strike the of rollover anticline (Figure 29 and Figure 30). Both the V-17 and V-19 intervals are affected by the rollover anticline structure as indicated by examination of the TWT maps (Figure 32 and Figure 33). The rollover anticline structure is located in the northern section of the study area. South of the rollover anticline the V-17 is dipping south towards the middle of the study area creating a syncline between

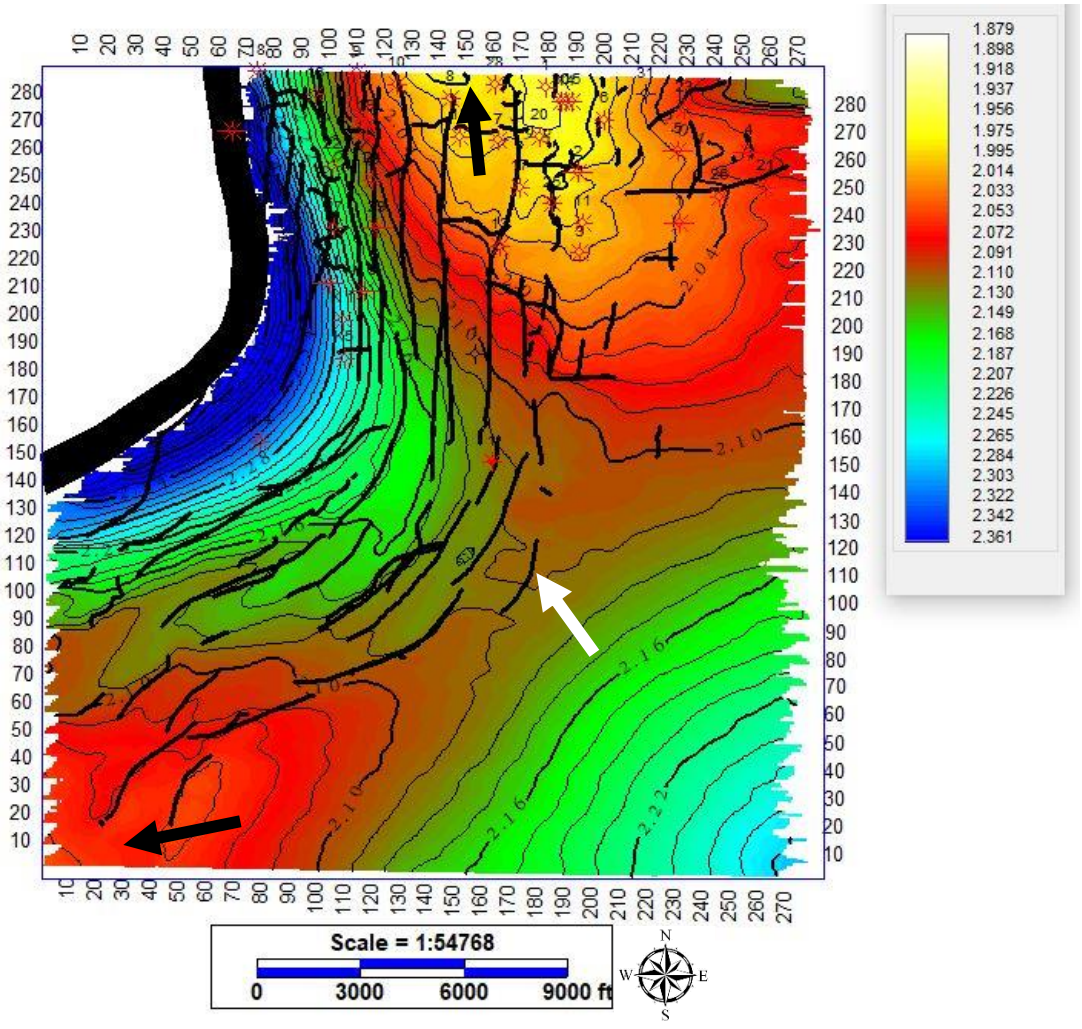

Figure 32: TWT map of the V-17 horizon (time in seconds). Structural highs are indicated by black colored arrows. A syncline is indicated by a white arrow.

structural highs (Figure 32). The V-17 is striking north-east south-west and the dip varies due to the VFZ producing the rollover anticline and the syncline. The TWT map of the V-19 verifies fault concentration is increasing with depth in the LOVF (Figure 31, Figure 32, and Figure 33). The structure of the V-19 is striking north-east south-west, while the dip direction varies because of the main rollover anticline. West of the rollover anticline the interval is dipping towards the VFZ,

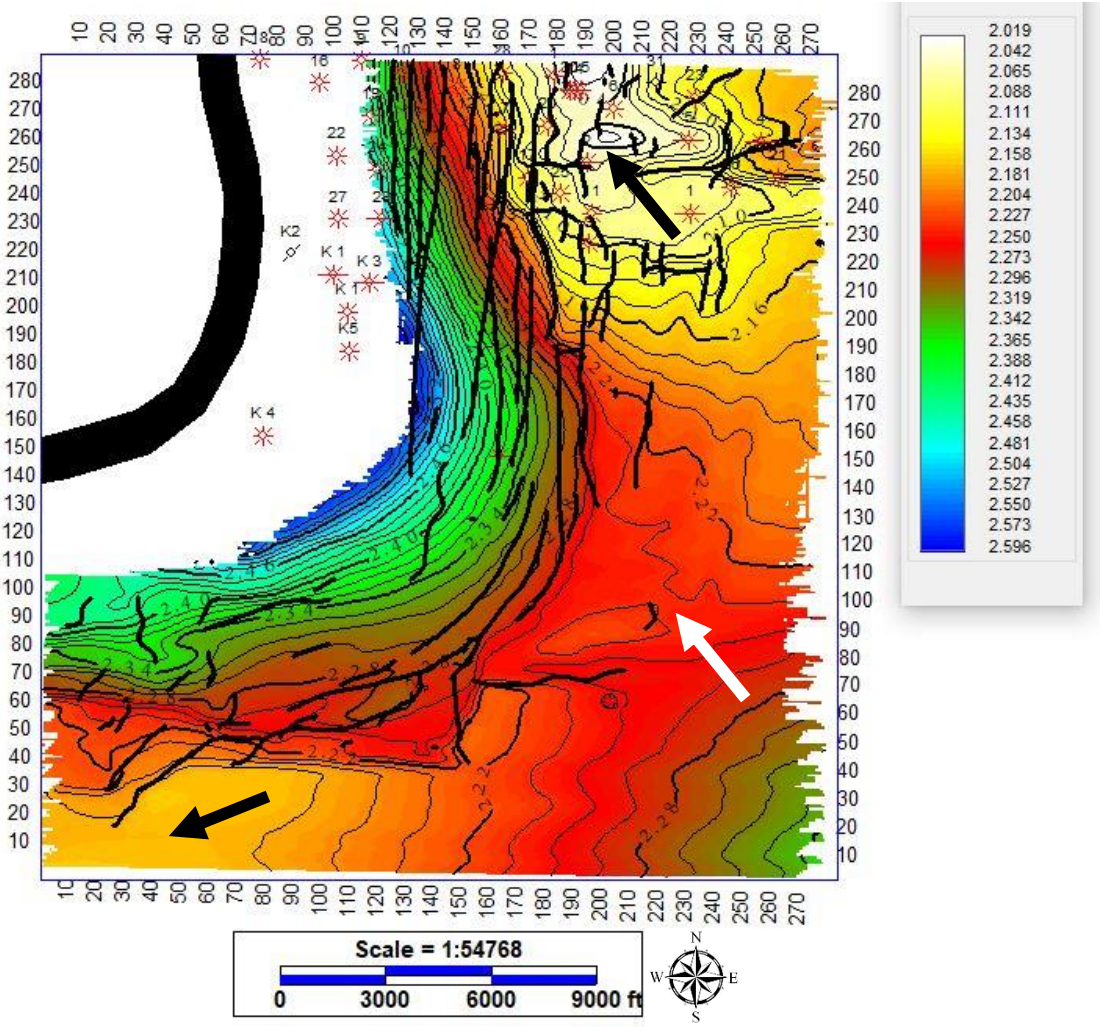

Figure 33: TWT map of the V-19 horizon. (time in seconds). Structural highs are indicated by black colored arrows and a syncline indicated by a white colored arrow.

on the eastern flank of the rollover anticline the interval is dipping east-southeast, and south of the rollover anticline the interval is dipping towards the syncline in the middle area of the 3D grid.

Two structural culminations can be seen within the TWT map; the rollover anticline and another high in the south-western portion of the grid. The VFZ is trending away from the southern section of the grid and no rollover anticline structure was developed due to the distance away from the VFZ. As all maps illustrate, fault clusters A and B trend with the VFZ and fault cluster C faults trend perpendicular to the strike of the rollover anticline (Figure 33).

Visualization of The Lower Vicksburg

An illustrative 3D visualization model, built in IHS Kingdom® VuPAK, displays the Eocene Jackson Shale glide plane with the overlying V-19, V-17, and V-102 sand intervals of the Vicksburg (Figure 34). This visualization displays how the VFZ and secondary faults have affected the sand reservoir intervals of the lower section of the LOVF. The Jackson Shale glide plane is the decollement surface upon which the LOVF is slipping. The V-19 overlies the glide plane, the V-17 overlies the V-19, and the V-102 overlies the V-17.

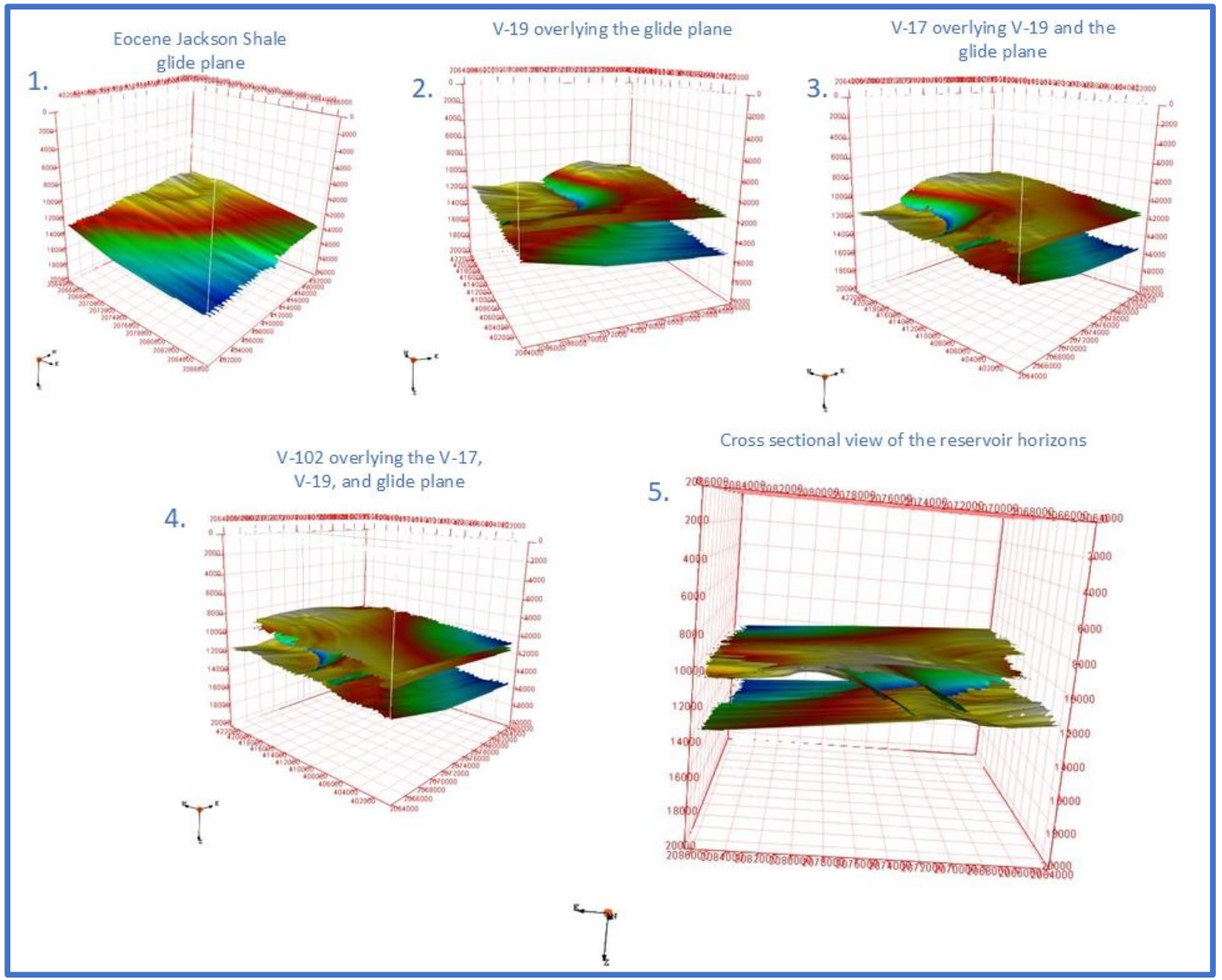

Figure 34: Visualization of the 3D cube displays the Eocene Jackson Shale glide plan along with overlying V-19, V-17, and V-102 (1-4). (5) displaying a cross sectional view of the horizons using IHS Kingdom® VuPAK®

Table 1: Production data for wells producing out of the V-102, V-17, and V-19 reservoirs (unit: million cubic feet [Mcf]). Annual gas production is calculated using cumulative gas production divided by the years producing.

API/UWI	Well/Lease Name	Well Number	First production	Last Production	Total gas production (Mcf)	Annual Gas production	Formation
42047300300000	BORGLUM, ANNA MARY, PETTUS	1	12/1/1970	8/1/1974	300,758	80202	V-102
42047307180000	CARTER RANCH	2	7/1/1979	5/1/2010	5,997,654	199922	V-19
42047306690000	CARTER RANCH	1	7/1/1979	8/1/1989	595,764	60607	V-19
42047309450000	CARTER RANCH	6	10/1/1981	12/1/1994	365720	28505	V-19
42047308460000	CARTER RANCH	5	7/1/1983	1/1/2017	2,224,127	72731	V-19
42047310630000	CARTER RANCH	7	8/1/1983	4/1/1997	4,239,977	553522	V-17
42047313490000	CARTER RANCH	8	7/1/1984	8/1/2020	7,915,402	228901	V-17
42047313940000	CARTER RANCH	9	1/1/1985	8/1/2020	3,543,201	120109	V-17
42047307360000	CARTER RANCH	3	8/1/1987	9/1/2012	1,119,903	44511	V-19
42047317880000	LA RUCIA RANCH	10	2/1/1998	8/1/2020	3,757,667	166416	V-17
42047318040000	LA RUCIA RANCH	11	9/1/1998	10/1/2016	656,288	36139	V-19
42047318730000	LA RUCIA RANCH	12	1/1/2000	8/1/2020	1,724,298	83461	V-17
42047319160000	LA RUCIA RANCH	14	4/1/2001	10/1/2007	367,606	63931	V-17
42047319060000	LA RUCIA RANCH	13	4/1/2001	8/1/2020	734,881	39383	V-17
42047321070000	LA RUCIA RANCH	16	12/1/2003	8/1/2020	5,444,901	325069	V-102
42047321210000	LA RUCIA RANCH	17	3/1/2004	2/1/2018	2,301,522	195874	V-17
42047321280000	LA RUCIA RANCH	18	5/1/2004	8/1/2020	701,433	43621	V-102
42047321390000	LA RUCIA RANCH	19	7/1/2004	8/1/2020	2,447,789	152987	V-102
42047321490000	LA RUCIA RANCH	20	9/1/2004	8/1/2020	2,715,959	169747	V-19
42047321610000	LA RUCIA RANCH	22	1/1/2005	8/1/2020	3,088,565	197290	V-102
42047321780000	LA RUCIA RANCH	24	3/1/2005	4/1/2020	2,258,543	156734	V-102
42047322290000	LA RUCIA RANCH	27	4/1/2006	8/1/2020	2,449,101	173204	V-102
42047322580000	LA RUCIA RANCH	28	5/1/2006	8/1/2020	1,019,619	71153	V-17
42047322660000	LA RUCIA RANCH	29	10/1/2006	9/1/2019	1,075,592	141899	V-102
42047323200000	LA RUCIA RANCH	30	1/1/2008	9/1/2017	3,459,859	388312	V-19
42047324770000	LA RUCIA	K 3	10/1/2012	12/1/2018	1,305,571	208891	V-102
42047324860000	LA RUCIA	K 4	7/1/2013	8/1/2020	3,204,530	457790	V-102
42047324830000	LA RUCIA	K 1	2/1/2019	8/1/2020	29,335	20805	V-102
42047324880000	LA RUCIA	K 5	2/1/2019	8/1/2020	20,111	14263	V-102
					Total gas production (Mcf)=62,617,887	Total annual gas production (Mcf) = 4,495,979	

Faults Control on The Hydrocarbon Accumulation

Synthetic, antithetic, and coast-perpendicular faults were interpreted, mapped, and investigated in order to describe the fault controls on the hydrocarbon reservoir accumulation and spatial distribution within the study area. The synthetic faults (those dipping east), antithetic faults (dipping west), and coast-perpendicular faults are migrating or trapping hydrocarbons reliant upon terminations against or breaches of the overlying shale seal layer seen between the V-102 and the V-16 horizons. The three key productive reservoir members within the study area are the V-102, V-17 and V-19. These intervals will be the focus of this section (Figure 35). Production data from wells targeting the V-102, V-17, and V-19 is listed in Table 1.

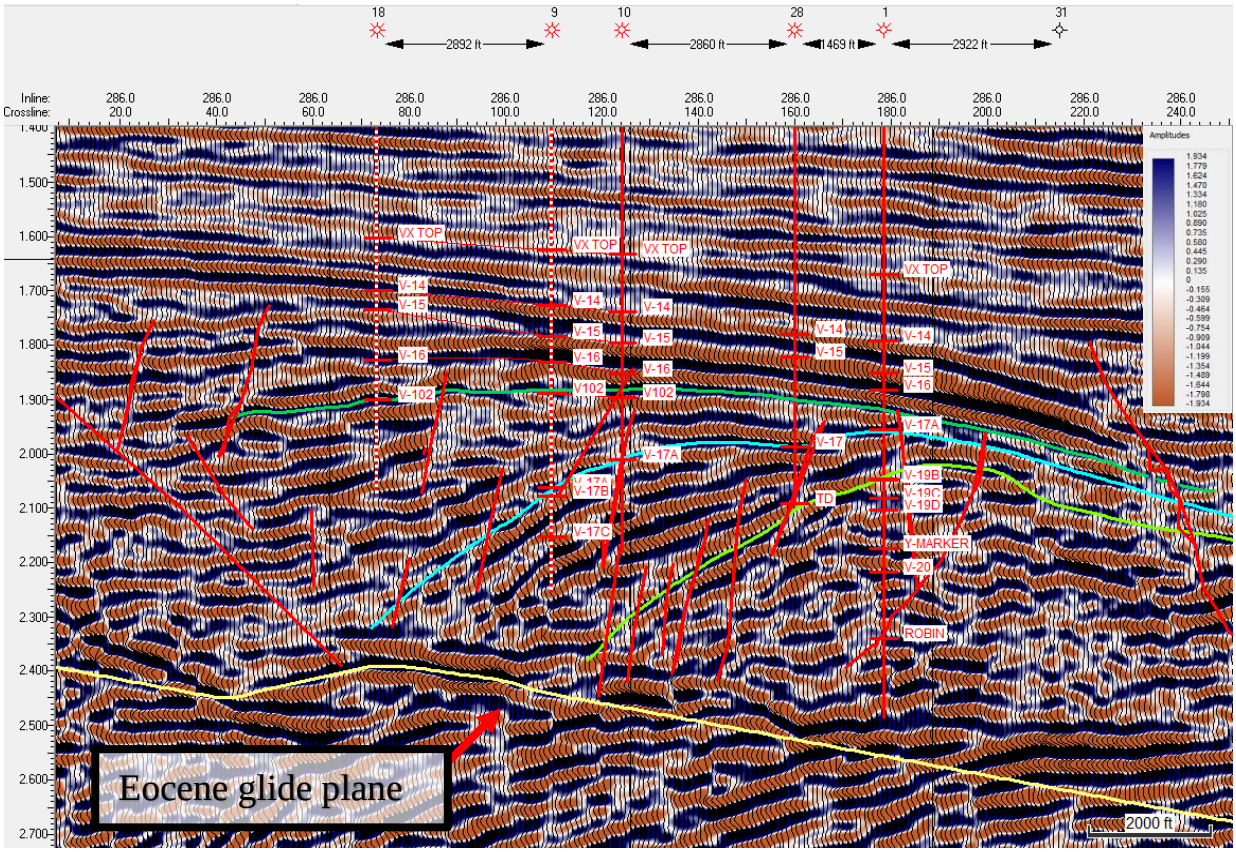

Figure 35: Seismic inline 266 displaying the V-102 (dark green), V-17 (light blue), and V-19 (light green) reservoir horizons within the rollover anticline.

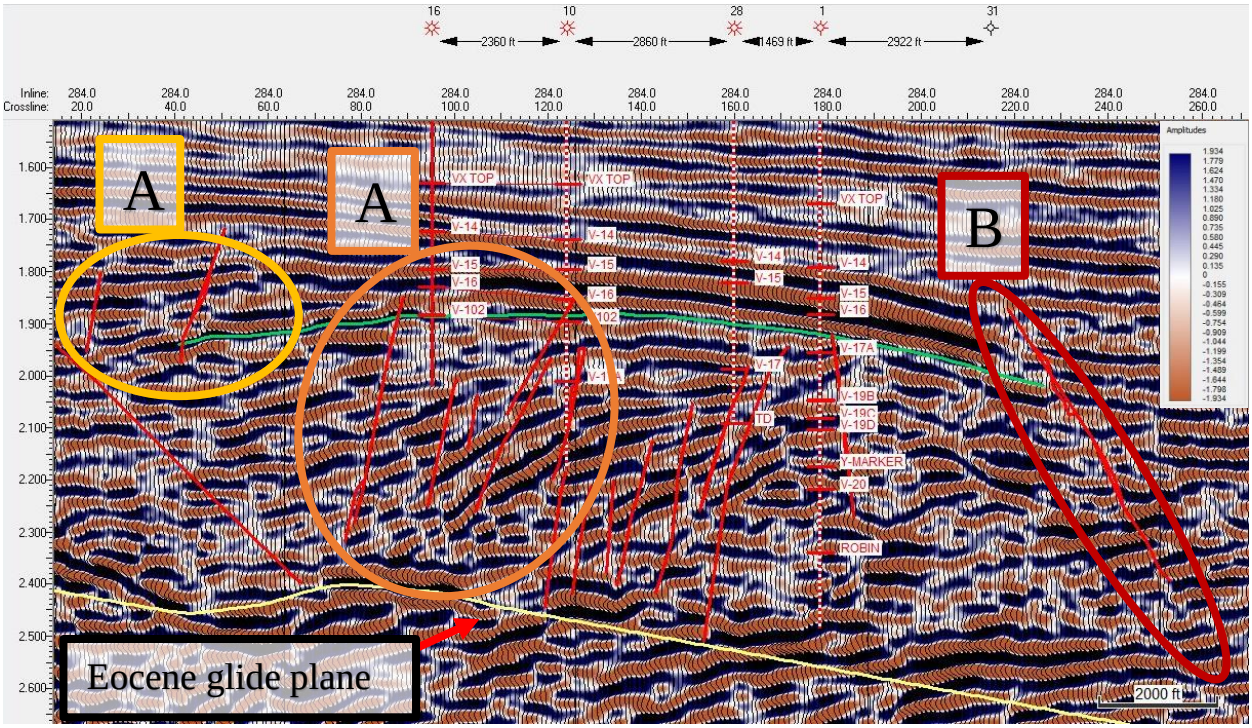

Figure 36: Seismic inline 284 displaying the V-102 interval and the fault clusters A (antithetic proximal to VFZ), A (antithetic faults proximal to rollover anticline), and B (synthetic fault). Location of seismic line marked by thin red transparent in Figure 37. Colored circles indicate fault clusters.

The V-102 horizon is affected by antithetic faults and accumulation within the V-102 reservoir depends on how the faults are affecting the overlying shale seal layer. The antithetic faults affecting the V-102 reservoir have been interpreted into two clusters A, and B (Figure 36). Cluster A antithetic faults are distal to the La Rucias Field rollover anticline and proximal to the major listric fault, and cluster B synthetic faults are proximal to the rollover anticline and distal to the listric fault. Cluster A faults are terminated by an unconformity before the overlying shale seal layer, except for cluster A faults located near the main VFZ. Cluster B faults are affecting the overlying shale seal layer, allowing enhanced migration of hydrocarbons upwards from the V-102 reservoir. Three large cluster B faults are key to the V-102 within the study area. Fault cluster A, proximal to the VFZ and cluster B, are allowing enhanced migration out of the V-102 reservoir (Figure 37).

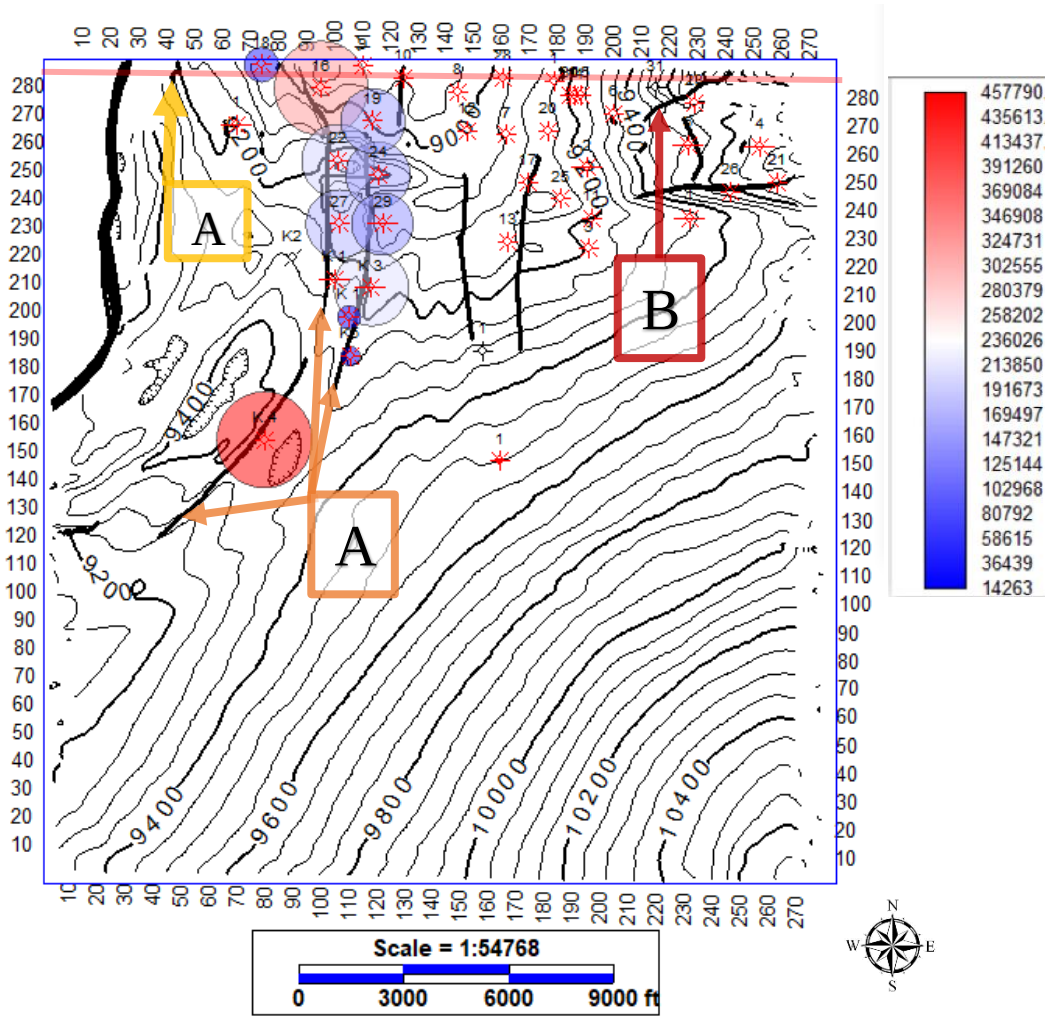

Figure 37: Structural depth map with colored bubble showing the average annual production rate (in Mcf) of wells producing from the V-102 interval. Fault clusters A and B are marked with colored arrows.

The V-17 horizon is impacted by synthetic, antithetic, and coast-perpendicular faults. Antithetic faults (cluster A) on the western flank of the rollover anticline are terminating beneath the shale seal layer allowing accumulation within the V-17 reservoir (Figure 38 and Figure 39). Synthetic faults (cluster B) are located on the western flank of the rollover anticline and are affecting the overlying shale seal layer, allowing migration of hydrocarbons out of the V-17 reservoir. Coast-perpendicular faults combined with antithetic faults (bi-directional) are also allowing enhanced migration, and accumulation of hydrocarbons within the V-17. The most

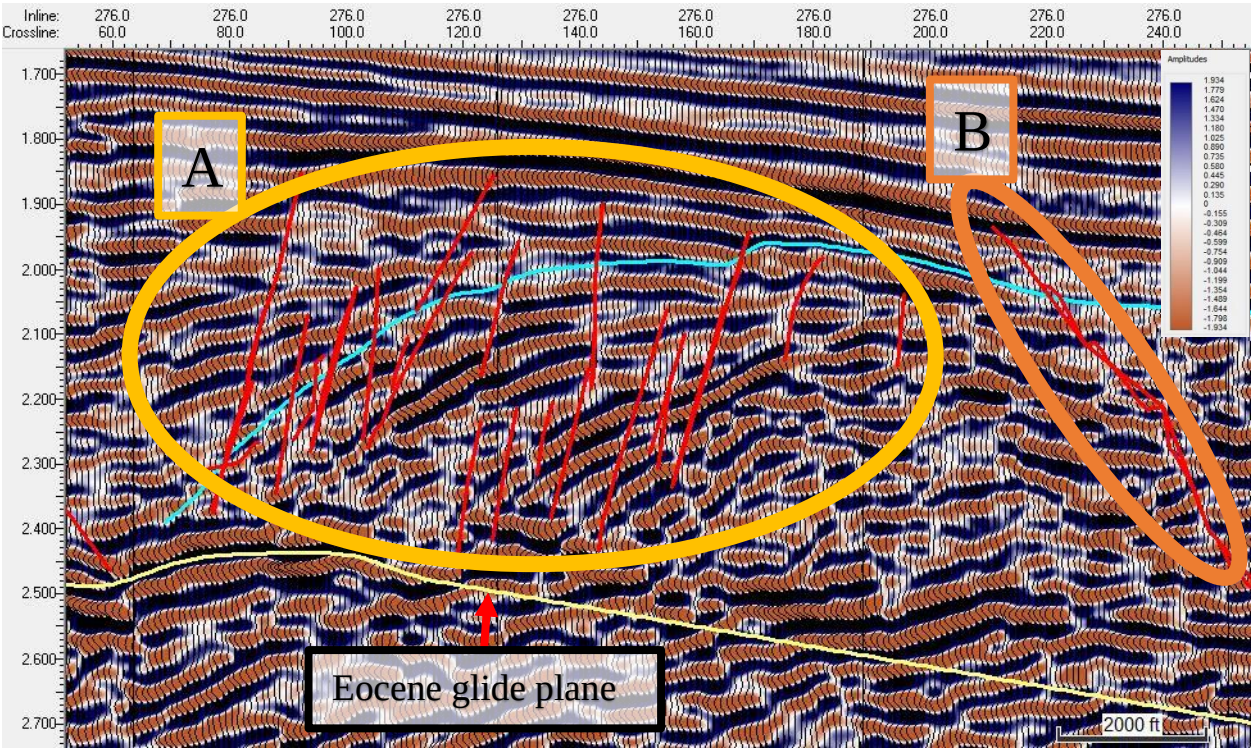

Figure 38: Seismic inline 276 displaying the V-17 interval (cyan Blue) within the rollover anticline structure. Fault clusters A (antithetic faults) and B (synthetic faults) shown in colored circles. Location of seismic inline marked by thin red transparent line in Figure 39.

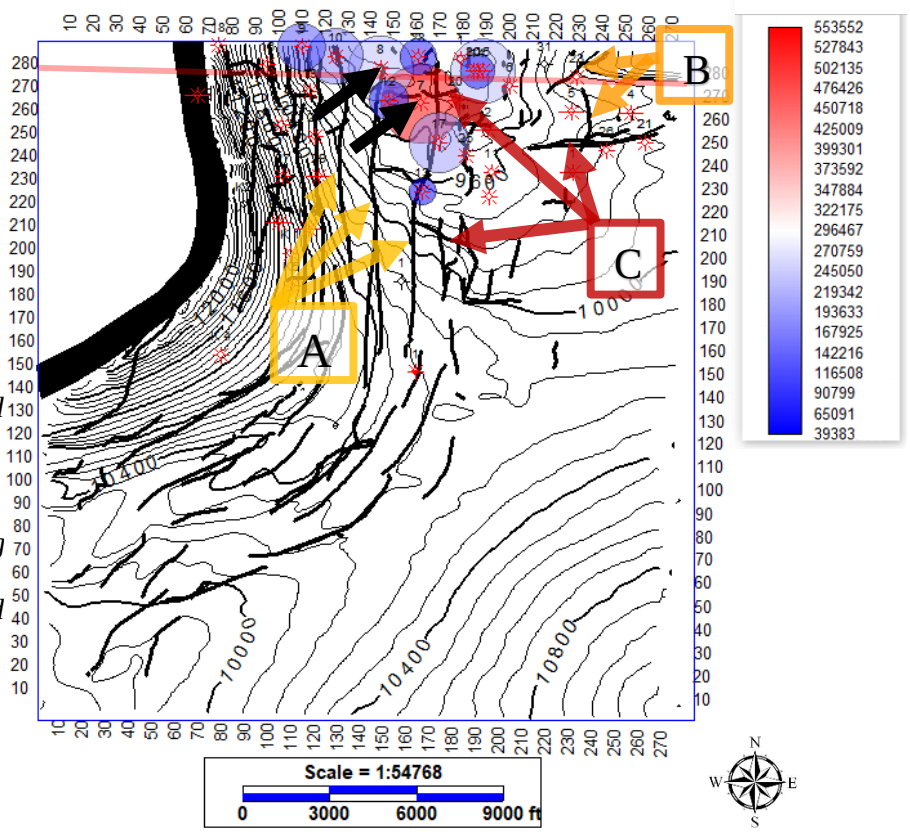

Figure 39: Structural depth map with colored bubble showing the average annual production rate (in Mcf) of wells producing from the V-17 interval. Fault clusters A, B, and C are marked with colored arrows.

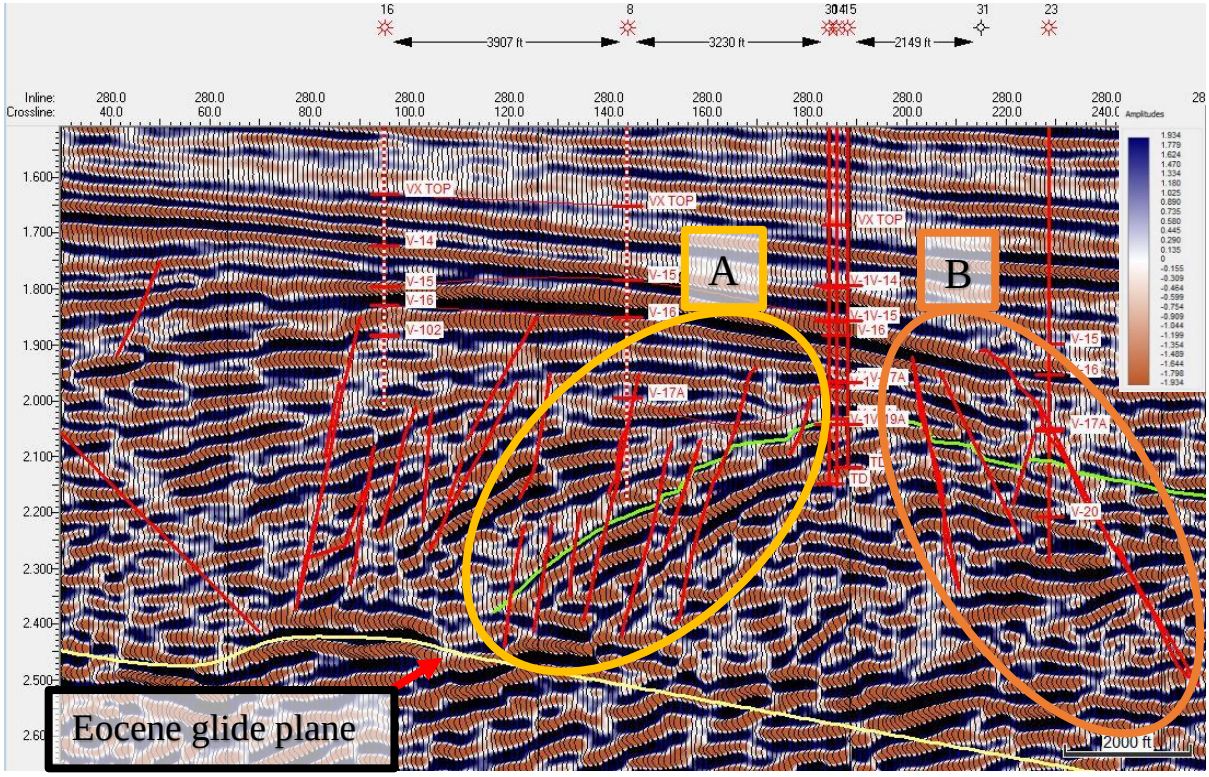

Figure 40: Seismic inline 280-displaying the V-19 interval (light green) with fault clusters A (Antithetic faults) and B (Synthetic faults). Location of seismic line marked by thin red transparent line in Figure 44: Structural depth map with colored bubble showing the average annual production rate (in Mcf) of wells producing from the V-19 interval. Fault clusters A, B, and C are

productive wells within the study area are hydrocarbon charged by bi-directional faulting, (wells La Rucia #7 and #8) (Figure 39).

The V-19 horizon is impacted by synthetic, antithetic, and coast-perpendicular faults. Synthetic faults located on the eastern flank of the rollover anticline are affecting the V-19 reservoir and the overlying shale seal layer allowing for gas migration out of the V-19 reservoir. Meanwhile, the antithetic faults are terminating before the V-17 and/or before the overlying shale seal layer allowing accumulation within multiple horizons (V-19 and/or V-17) (Figure 40). The structural depth map in Figure 41 illustrates productive wells from the V-19 reservoir and fault

clusters impacting the V-19 interval. See Table 1 for specific historical well hydrocarbon production information.

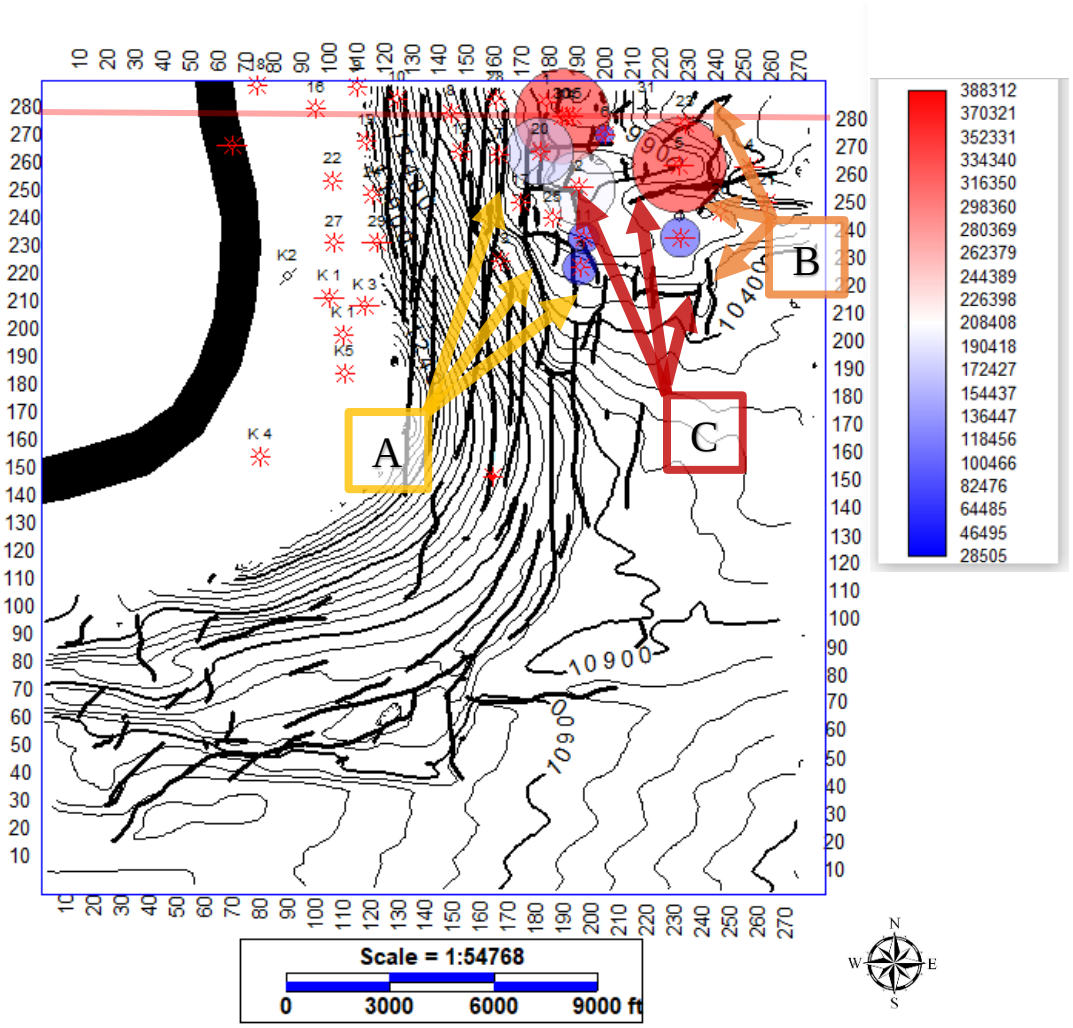

Figure 41: Structural depth map with colored bubble showing the average annual production rate (in Mcf) of wells producing from the V-19 interval. Fault clusters A, B, and C are marked with colored arrows.

Conceptual Model

A conceptual model has been developed to provide a prospective of the complex structural and stratigraphic controls on hydrocarbon accumulation within the La Rucias Field. This model integrates structure, fault geometry, stratigraphy, and production data (Figure 42). This conceptual

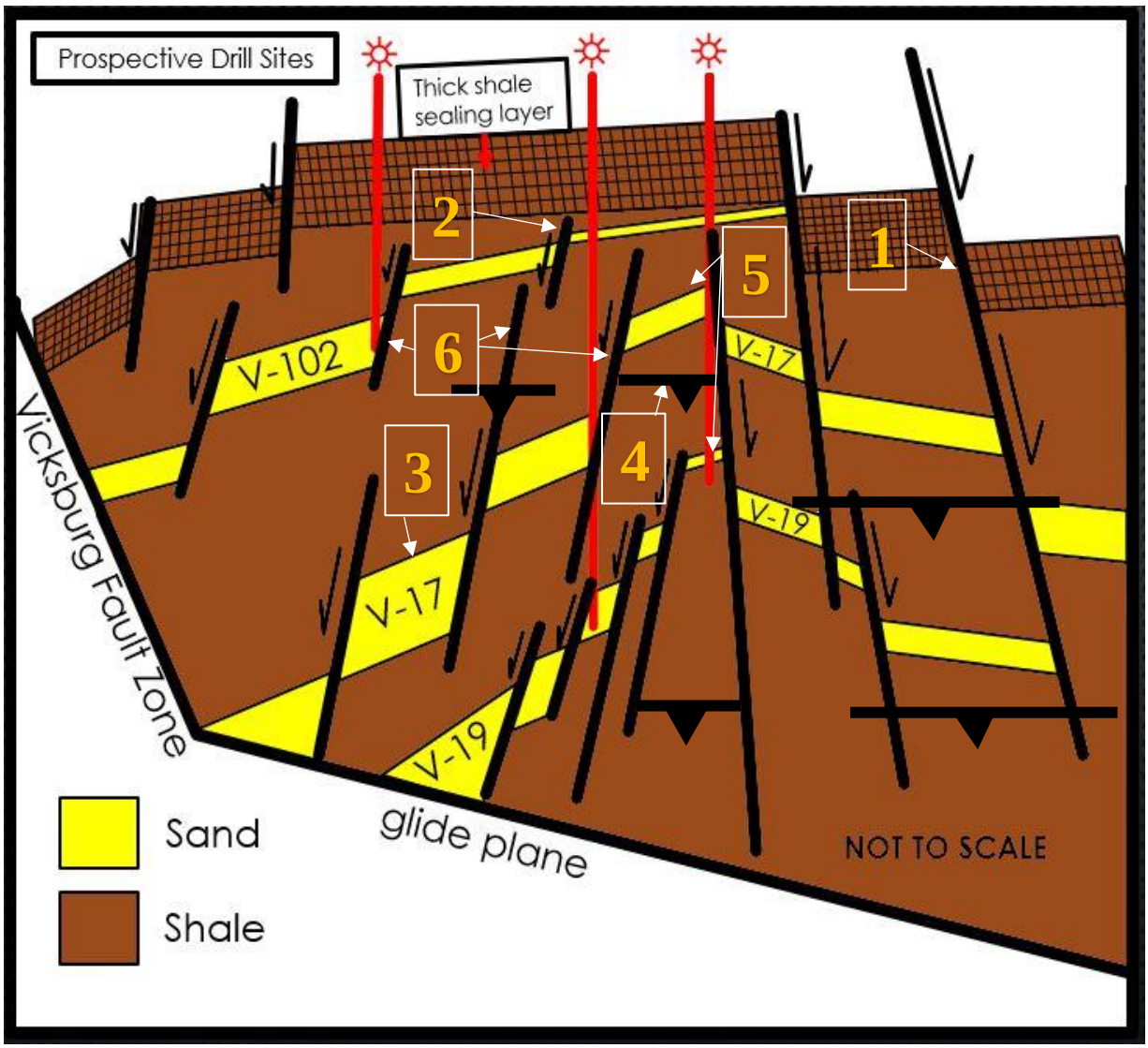

Figure 42: Conceptual model of structural and stratigraphic controls affecting hydrocarbon accumulation within the V-102, V-17, and V-19 reservoirs. Cluster C faults depicted as horizontal black lines with triangles.

model indicates that: (1) faults affecting any of the reservoir members (V-102, V-17, and V-19) and the overlying shale seal layer are acting as conduits rather than controls on trapping; (2) antithetic faults displacing any of the reservoir members (V-102, V-17, and V-19) and terminating

before the overlying shale seal layer are acting as traps and allowing accumulation of hydrocarbon with the affected reservoir member; (3) where antithetic faults produce sufficient throw on the downthrown block, a lateral seal can form, creating more favorable conditions for accumulation of hydrocarbons; (4) intersecting fault systems (parallel and perpendicular to regional southwest-northeast Gulf Coast) act as conduits rather than traps and these provide additional pathways for gas migration into the V-17 and V-19 sand reservoirs; (5) the fault control is specific to the location and geometry of the rollover anticline; and (6) additional productive well locations could target the western-dipping faults seen in the V-102, V-17, and V-19 reservoir members (Figure 42).

CHAPTER IV

Discussion and Conclusion

The Lower Oligocene Vicksburg Formation of the coastal plains of Texas has been thoroughly investigated for hydrocarbon exploration throughout the decades. Paralic sand complexes (deltas, delta flanks, and associated shorezones) with alternating sand and shale assemblages dominate the lower section and upper section of the Vicksburg Formation (Coleman et al., 1990). The lower section of the LOVF is highly influenced by syndepositional listric faults through a low-stand systems tract that initiated syndepositional faulting by infilling tremendous quantities of sediment on the down thrown block of the listric fault and developing rollover anticlines, and secondary fault systems.

This master's thesis study provides a thorough investigation of how secondary faults, those related to the major listric fault, are affecting the lower, middle, and upper delineations of the Vicksburg Formation and how faults control gas accumulations in the reservoir members of the LOVF (e.g., V-102, V-17, and V-19). A more thorough analysis of fault control could be aided by investigating the internal seals within the V-17 and V-19 reservoir intervals. Furthermore, how are structural features associated with mini-subbasins developed by coast-perpendicular faults associated with convergence of differential down slope movement of the La Rucias Field and the northern La Rucias Field? These topics are considered in the next sections as well as a qualitative assessment of faults picked from amplitude maps.

Internal Seals Within The V-17 And V-19

Establishing the role of controls on reservoir accumulation can be accomplished by investigating the petrophysics of V-17 and V-19 internal seals. These internal seals in combination with secondary faults could be providing an additional combination of structural and stratigraphic

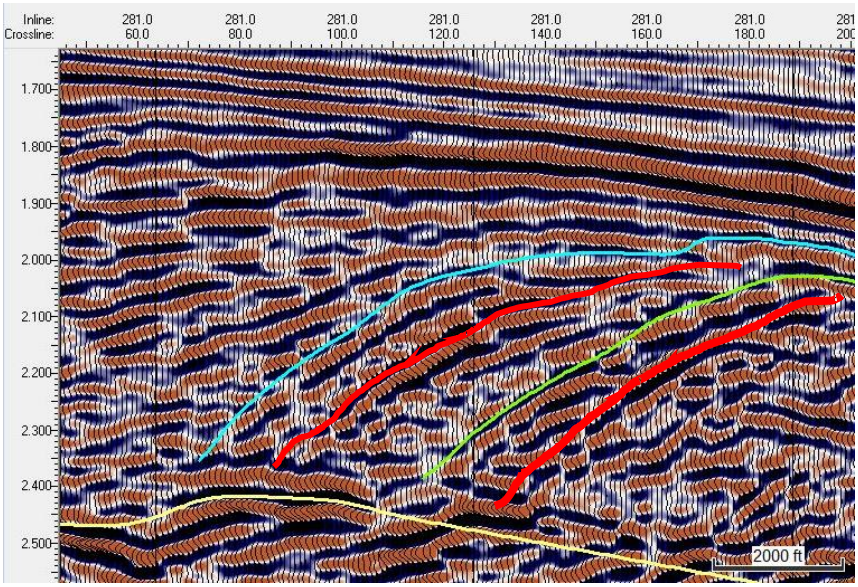

Figure 43: Seismic inline 281 showing the V-17 (light Blue) and V-19 (light green) intervals. Possible locations of internal seal zones are marked with red lines.

traps within the V-17 and V-19 intervals. Figure 43 illustrates possible internal seal zones based upon an alternating sand-shale assemblage. Depending on the size and spatial distribution of the seal layers, fault clusters could displace the internal seals to create a barrier to fluid flow, allowing accumulation within the V-17 and V-19 reservoirs. The lower section of the Vicksburg Formation is highly-pressurized (0.94 psi/ft [21.2 kPa/m]) and compartmentalized; (Berg et al., 1982), bounded by the lower Eocene Jackson Shale below and the unconformity above, separating the lower section from the upper section of the Vicksburg. The pressurization is largely due to clay transformation and hydrocarbon generation (Berg et al., 1982). The median mud weight used to drill within southern Brooks county can be as high as 17.5 pounds per gallon (ppg) to 18.5 ppg (Hoover et al., 2008). The upper section is bound above by the upper Frio Catahoula formation

and the lower unconformity (Al-Shaieb et al., 2000). To investigate internal seals, fluid inclusion stratigraphy and micro imaging logs could be integrated into the study. Fluid inclusions are usually abundant within internal seals due to high cementation within the seal zone (Al-Shaieb et al., 2000). Mapping these seal zones would add additional data as to how the faults are affecting the V-17 and V-19 internal seals.

Origin of Coast Perpendicular Faulting

Coast-perpendicular faulting within the study area has had a significant effect on gas accumulation and migration. Shale diapirs can create mini subbasins (Ogiesoba et al., 2018;

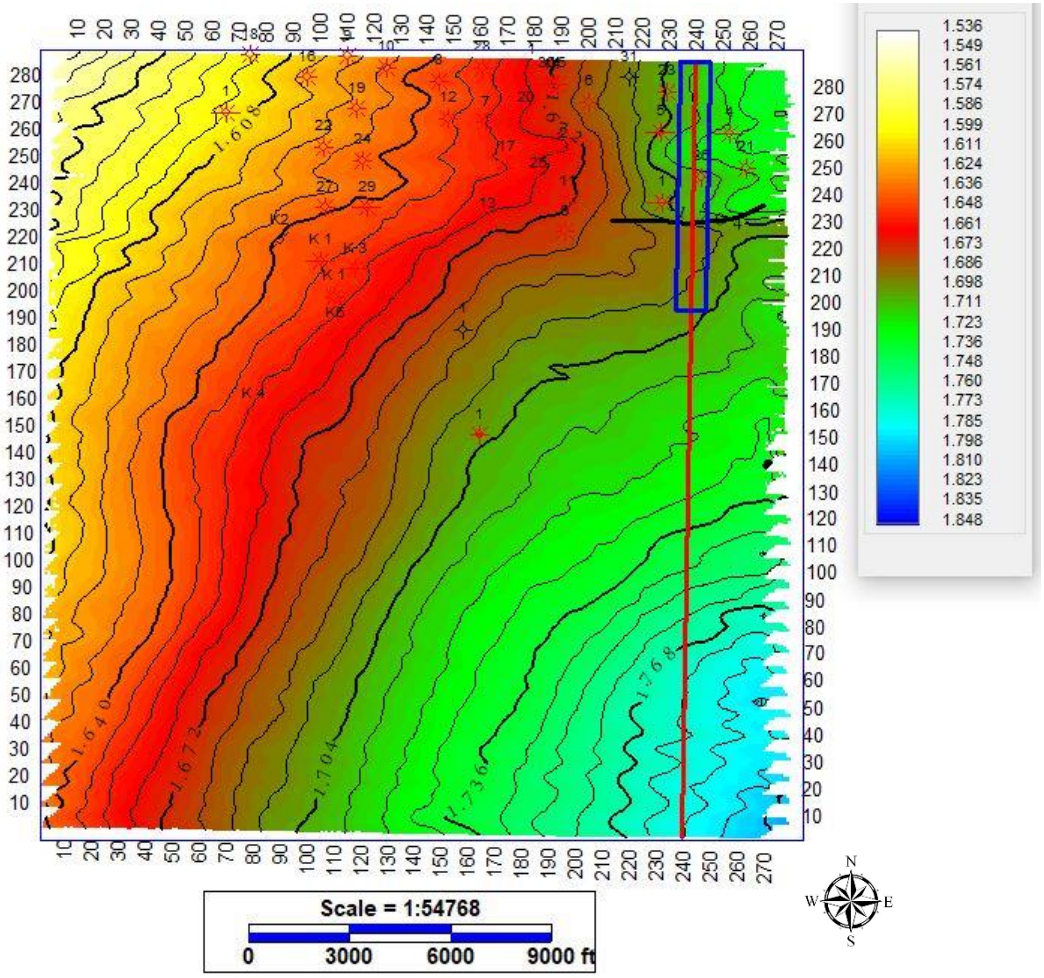

Figure 44: TWT map of the VX-Top interval with large coast perpendicular fault shown in the northeastern section of the grid and the location Figure 44 marked by thin red line and blue rectangle.

Treviño et al., 2008) and can initiate coast-perpendicular faulting. An extensive and regionally important coast-perpendicular fault has been observed in the north eastern section of the study area, east of the rollover anticline (Figure 44).

The coast-perpendicular fault seen in Figure 45 is affecting the lower, upper, and middle sections of the Vicksburg Formation. This is the only fault within the study area that cuts across all investigated intervals; thus, the fault is believed to be associated with a major coast-perpendicular wrench fault. To investigate the possible wrench fault associated with shale diapirs,

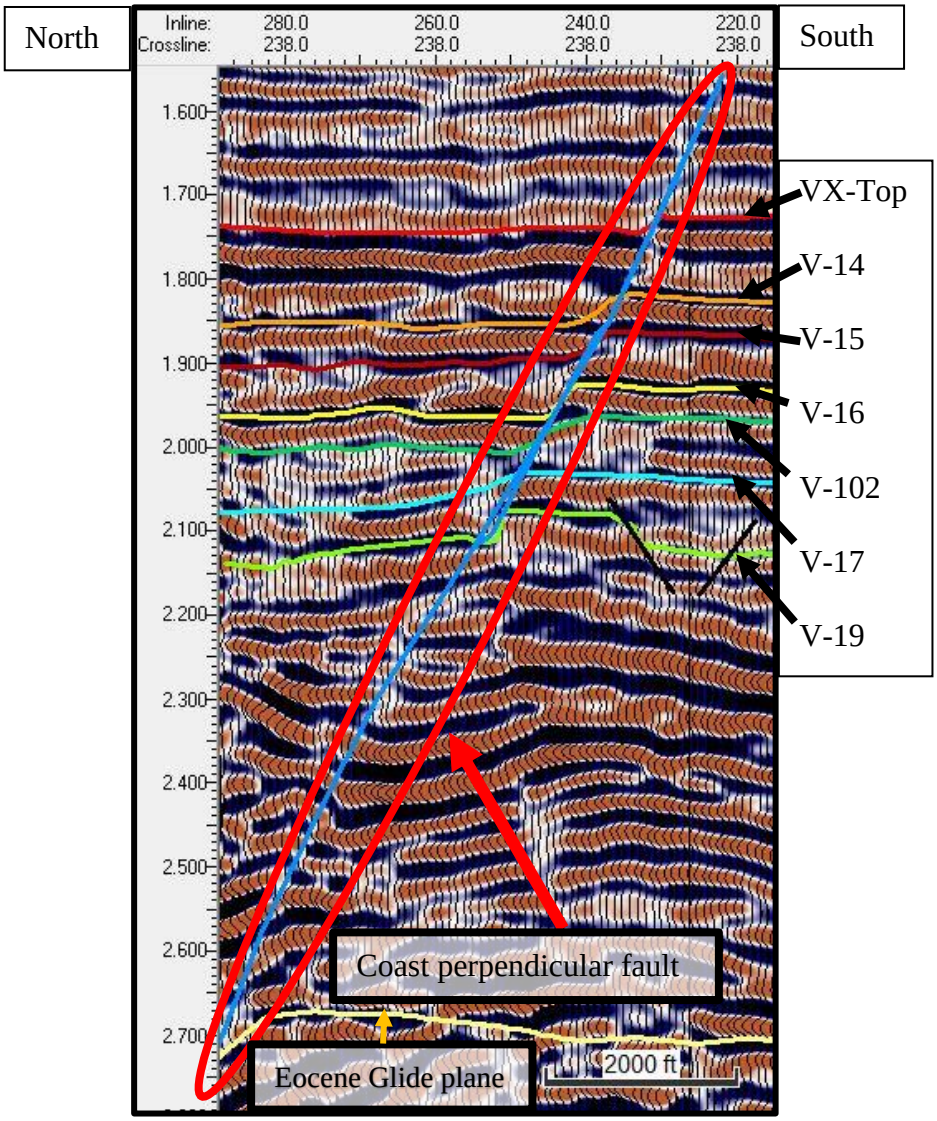

Figure 45: Seismic crossline 238 displaying large coast perpendicular fault (circled in red).

an additional 2D seismic line was donated by SEI to further investigate fault seal potential and the structural relationships between the southern La Rucias field and the Northern La Rucias field.

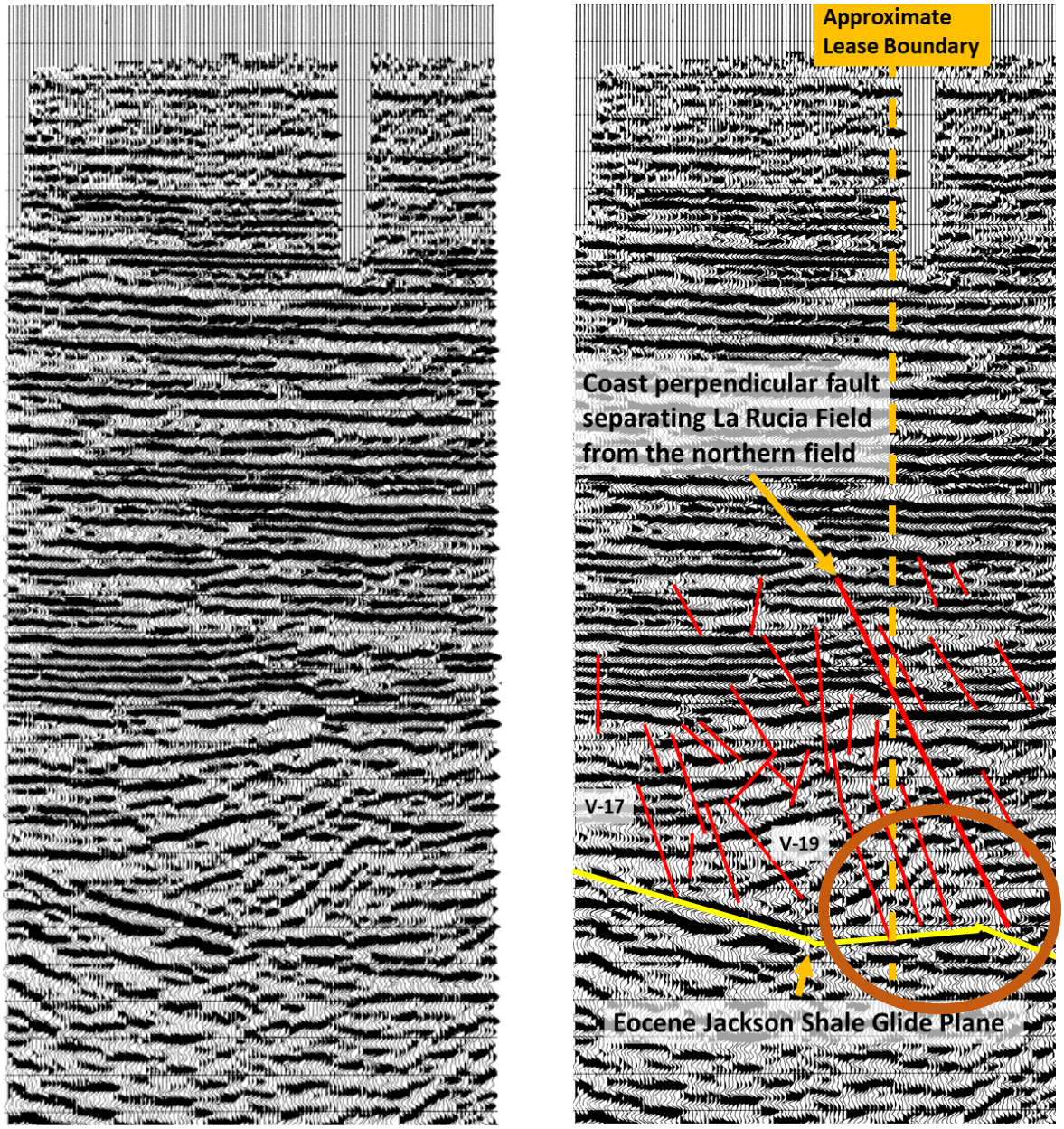

Figure 46: 2D seismic line extended outside our study area, left is the uninterpreted section; right shows interpreted faults shown in red and the coast perpendicular wrench fault and approximate lease line. Possible shale diapir indicated by brown circle. Seismic data owned or controlled by Seismic Exchange, Inc; interpretation is that of Ryan Turner

Interpretation of the 2D seismic profile, extended outside the study area, suggests a coast-perpendicular wrench fault dipping north is separating the southern La Rucias Field (Carter Ranch

Lease) from the northern La Rucias Field (Lopez Ranch Lease) (Figure 46). The left-lateral slipping fault extends from the Eocene glide plane through the Vicksburg and into the above Frio Catahoula Formation. The origin of the coast-perpendicular fault is most likely associated with differential down-slope movement of the southern La Rucias Field and the northern La Rucias Field. These fields are affected by small amounts of convergence on the hanging-wall structural

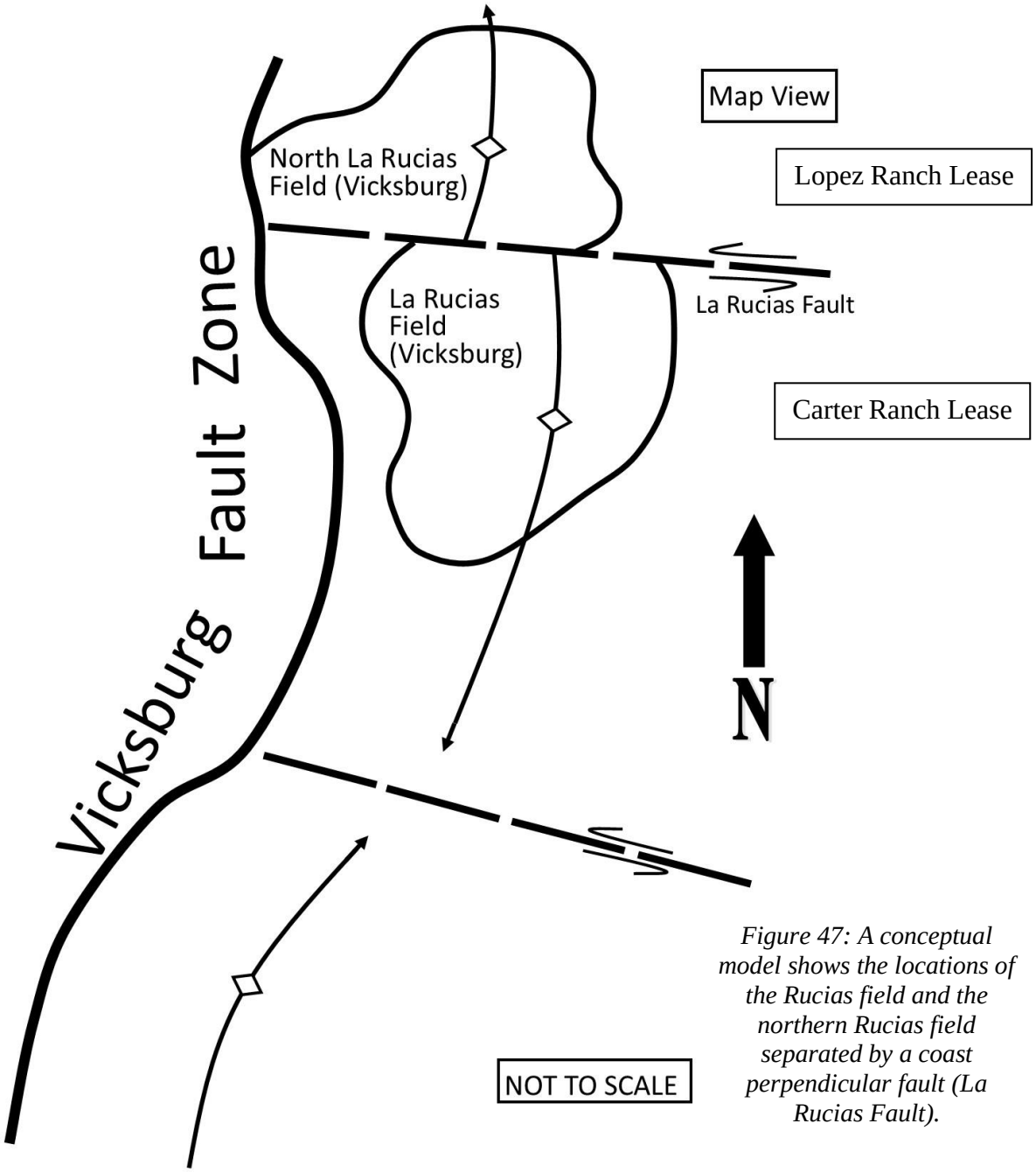

Figure 47: A conceptual model shows the locations of the Rucias field and the northern Rucias field separated by a coast perpendicular fault (La Rucias Fault).

block of the listric fault. This is likely due to the listric fault running through the fields, creating a u-shape structure. The displacement vectors of the fields are convergent and a subsequent shale ridge develops (Treviño et al., 2008). A spatial model was developed to illustrate how the wrench fault may be displacing the La Rucias Fields (Figure 47). The model shows how the La Rucias fields are separated from one another with left-lateral offset. The wrench fault is likely sealing off the fields from communicating with each other. Additional and better-quality 3D seismic data would be needed to study the wrench fault to infer shale sealing potential within the fault.

Qualitative Assessment of Fault Picking

Faults affecting reservoir intervals were cross-referenced with amplitude maps (Figure 48). Amplitude maps allow the interpreter to initiate a qualitative assessment of any overlooked faults seen on seismic lines. The maps are constructed by the interpreter in regular workflow. Slight variation within the seismic reflection cannot be seen by the interpreter during fault interpretation on seismic lines. Slight change in amplitude shown in map view can indicate a coast perpendicular fault is present and sufficiently imaged to be interpreted.

Faults suggested from the amplitude maps were correlated with those extracted from seismic in-lines and crosslines (Figure 49). Examination of Figure 48 and Figure 49 illustrates a match between the negative amplitudes, seen as white strips trending with the VFZ and the overlying faults. Fault clusters A (antithetic) and B (synthetic) are interpreted in inlines, while the cluster C faults are detected using the crosslines. The crosslines cut perpendicular through the fault surface allowing ready picking and interpretation. This integration method allows the interpreter to qualitatively assess cluster C faults to improve interpretation of hard to detect cluster C faults.

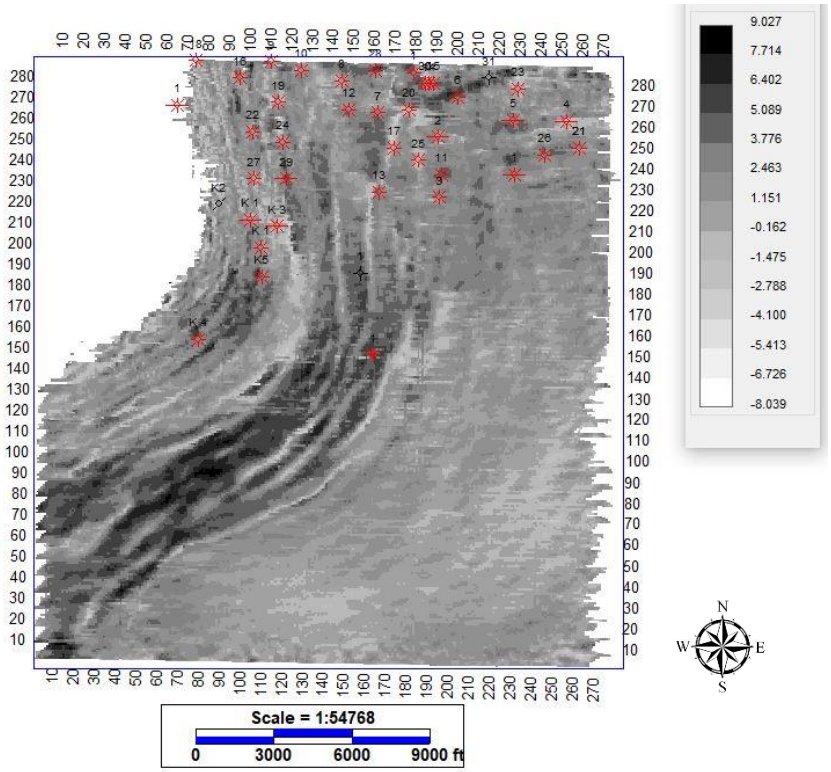

Figure 48: Seismic amplitude map of the V-17 with trends of low amplitude sections indicated faults affecting the horizon.

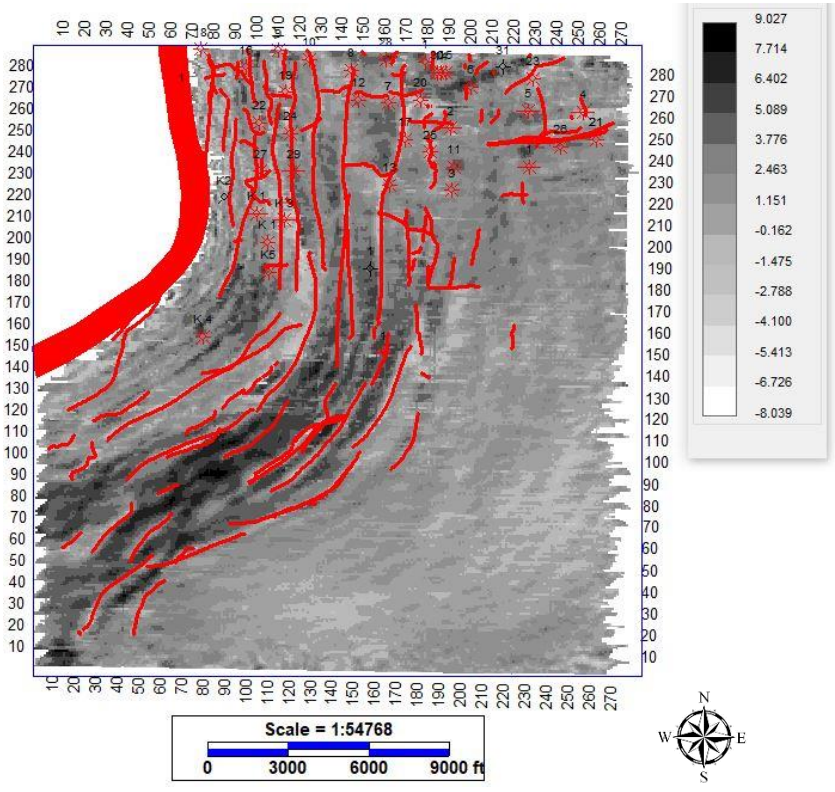

Figure 49: Amplitude map of faults overlying trends of low amplitude.

Conclusion

The La Rucias Field located in southern Brooks County is a prolific gas field producing hydrocarbons from several named sand reservoir intervals (V-102, V-17, and V-19) within the lower most section of the Lower Oligocene Vicksburg Formation (LOVF). The Vicksburg Fault Zone, striking northeast-southwest through the study area has highly influenced the LOVF. The syndepositional listric fault developed a rollover anticline, expanding the strata on the down thrown block of the listric fault and producing dilated alternating sand-shale reservoir intervals (V-102, V-17 and V-19).

Secondary faults affecting the lateral distribution of the V-102, V-17, and V-19 reservoirs trend with the listric fault. Perpendicular, striking north-south through the rollover anticline, these secondary faults are extremely complex. Interpreting and mapping secondary faults that are affecting the reservoir intervals has been essential to resolving fault control on reservoir accumulation and spatial distribution of hydrocarbons. Secondary faults affecting the reservoir intervals were assembled into three categories: cluster A (antithetic), cluster B (synthetic), and cluster C (coast perpendicular) faults. The fault clusters act as conduits allowing migration of gas into the reservoir intervals. The overlying and regional shale seal layer accumulate gas on the structure. If the overlying shale seal layer is faulted, the gas will migrate out of the lower section into the upper section of the LOVF. Fault clusters behave differently as the fault architecture is defined by antithetic faults on the western flank of the rollover anticline, synthetic faults on the eastern flank of the rollover anticline, and coast-perpendicular faults distributed throughout the rollover anticline. A cluster of antithetic and coast-perpendicular faults act as additional conduits for hydrocarbons to migrate into the reservoir intervals. The most productive well within the V-17 interval, Carter Ranch #7 (API 42047310630000 McCormick Operating Company) is located on

the structural high and is affected by bidirectional faulting, producing over 4.2 billion cubic feet (Bcf) of gas with an average annual production of 553,522 (Mcf) .

The identified controls on spatial distribution of hydrocarbons within the La Rucias Field is dependent upon the reservoir being targeted. The producing zones for the V-102, V-17, and the V-19 are spatially affected by secondary faults: The V-102 producing reservoir is located west of the rollover anticline and controlled by cluster A faults. The V-17 reservoir is on the western flank of the rollover anticline and is controlled by a combination of cluster A and C faults forming additional conduits for gas migration and accumulation. Here, cluster B faults are cutting through the overlying shale seal layer allowing enhanced migration above the V-17. The V-19 is on the central to eastern flank of the anticline controlled by clusters A and C, allowing migration and accumulation of gas within the V-19. Cluster B faults cut through the overlying shale seal layer, allowing enhanced migration above the V-19.

Future work in the study area would include petrophysical and stratigraphic investigation of internal seal layers within the V-102, V-17 and V-19 using micro imaging logs and fluid inclusion stratigraphy. The internal seal layers within the reservoir horizons act as barriers to fluid flow, in combination with the known controls of secondary faults. A further study would provide a better understanding of vertical compartmentalization of reservoir intervals and accumulation estimates within the La Rucias Field. The addition of 3D seismic data in the northern La Rucias Field would be used to further investigate the origin of the coast-perpendicular fault separating the southern La Rucias Field from the northern La Rucias Field and would provide insight to possible shale tectonics affecting the study site and producing mini basins on either side of the coast-perpendicular wrench fault. This would provide further evidence of controls on sediment loading,

sand distribution, structural development of the rollover anticline, and an improved assessment of reservoir accumulation and hydrocarbon spatial distribution within the La Rucias Field area.

REFERENCES

Al-Shaieb, Z., Puckette, J. (2000) Identification and characterization of reservoirs and seals in the Vicksburg, Formation, TCB field, Kleberg, County, Texas. Searchanddiscovery.Com. Retrieved from http://www.searchanddiscovery.com/documents/zuhair/index.htmZuhair

Asquith, G., Krygowski, D., Henderson, S., Hurley, N. (2004). Basic well log analysis. Basic well log analysis. American Association of Petroleum Geologists. https://doi.org/10.1306/mth16823

Bailey, W., Manzocchi, T., Walsh, J. J., Keogh, K., Hodgetts, D., Rippon, J. (2002). The effect of faults on the 3D connectivity of reservoir bodies: A case study from the East Pennine Coalfield, UK. Petroleum Geoscience, 8. https://doi.org/10.1144/petgeo.8.3.263

Bense, V. F., Gleeson, T., Loveless, S. E., Bour, O., Scibek, J. (2013). Fault zone hydrogeology. Earth-Science Reviews, 127, 171–192. https://doi.org/10.1016/j.earscirev.2013.09.008

Berg, R. R., Habeck, M. F. (1982). Abnormal Pressures in the Lower Vicksburg, McAllen Ranch Field, south Texas. Gulf Coast Association of Geological Societies Transactions Vol. 32 (1982), Pages 247-253

Bose, S., Mitra, S. (2012). Controls of listric normal fault styles in the northern Gulf of Mexico: Insights from experimental models. Marine and Petroleum Geology, 35(1), 41–54. https://doi.org/10.1016/j.marpetgeo.2012.01.012

Brown, L. F., Loucks, R. G., Trevino, R. H., Hammes, U. (2004). Understanding growth-faulted, intraslope subbasins by applying sequence-stratigraphic principles: Examples from the south Texas Oligocene Frio Formation. AAPG Bulletin, 88(11), 1501–1522. https://doi.org/10.1306/07010404023

Coleman, J. C., & Galloway, W. E. (1990). Petroleum Geology of the Vicksburg Formation, Texas: Abstract. AAPG Bulletin. https://doi.org/10.1306/20b22ff3-170d-11d7-8645000102c1865d

Combes, J. M. (1993). The Vicksburg Formation of Texas, Depositional Systems Distribution, Sequence Stratigraphy, and Petroleum Geology. The American Associtation of Petroleum Geologists Bulletin, 77(11), 1942–1970.

Ewing, T. E. (1991). Structural framework. In The Gulf of Mexico Basin (pp. 31–52). Geological Society of America. https://doi.org/10.1130/dnag-gna-j.31

Fazli Khani, H., Back, S. (2015). The influence of differential sedimentary loading and compaction on the development of a deltaic rollover. Marine and Petroleum Geology, 59, 136–149. https://doi.org/10.1016/j.marpetgeo.2014.08.005

Gaullier, V., Vendeville, B. C. (2005). Salt tectonics driven by sediment progradation: Part I - Mechanics and kinematics. AAPG Bulletin, 89(8), 1071–1079. https://doi.org/10.1306/03310503063

Han, J. H. (1980). Deltaic Systems and Associated Growth Faulting of Vicksburg Formation (Oligocene), South Texas: ABSTRACT; Depositional and Tectonic Evolution of a Basement-Bounded, Intracratonic Basin, Palo Duro Basin, Texas: ABSTRACT. AAPG Bulletin (Vol. 64). American Association of Petroleum Geologists. Retrieved from http://archives.datapages.com/data/bulletns/1980-81/data/pg/0064/0005/0700/0717.htm

Hoover, E., Trenery, J. (2008). High-Performance WBM Optimizes Drilling Efficiency In Demanding Vicksburg Wells | Cover Story | Magazine. Retrieved November 6, 2020, from https://www.aogr.com/magazine/cover-story/high-performance-wbm-optimizes-drilling-efficiency-in-demanding-vicksburg-w

Hosman, R. L. (1996). Regional stratigraphy and subsurface geology of Cenozoic deposits, Gulf Coastal Plain, south-central United States. Washington: U.S. G.P.O.

Kosters, E. C., Finley, R. J., Gas Research Institute., & University of Texas at Austin. (1989). Atlas of major Texas gas reservoirs. Chicago, Ill: Gas Research Institute.

Ogiesoba, O. C., Eluwa, A. K. (2018). Structural Styles of Eocene Jackson and Oligocene Vicksburg Formations within the Rio Grande and Houston Embayments near the San Marcos Arch , Refugio and Calhoun Counties , South Texas Gulf Coast, Gulf Coast Association of Geological Societies Transactions. Vol. 68 (2018), pg. 357–370.

Posamentier, H. W., Jervey, M. T., Vail, P. R. (1988). Eustatic Controls on Clastic Deposition I—Conceptual Framework. (C. K. Wilgus, B. S. Hastings, H. Posamentier, J. Van Wagoner, C. A. Ross, & C. G. S. C. Kendall, Eds.), Sea-Level Changes: An Integrated Approach. SEPM Society for Sedimentary Geology. https://doi.org/10.2110/pec.88.01.0109

Railroad Commission of Texas. Production Data. Retrieved January 7, (2020), from http://webapps2.rrc.texas.gov/ewa/productionqueryaction.do;jsessionid=etogxw5kp8lb6uboihwugv0bwpxjvvcu_ct8lorvcv8tfus0tne3!-926554712.

Reeher, L. (2017). Sequence Stratigraphy and Reservoir Characterization of the V17 Interval of the Vicksburg Formation (early Oligocene), Southern Brooks County, south Texas. UTSA. https://doi.org/10.1016/j.jenvman.2018.01.013

Saito, T., Bé, A. W. H. (1964). Planktonic Foraminifera from the American Oligocene. New Series (Vol. 145). Science (1964) 145(3633) 702-705 DOI: 10.1126/science.145.3633.702

Salvador, A. (1991). The Gulf of Mexico Basin. Boulder, Colo: Geological Society of America.

Shelton, J. W. (1984). Listric Normal Faults: An Illustrated Summary. American Association of Petroleum Geologists Bulletin, 68(7), 801–815. https://doi.org/10.1306/ad461426-16f7-11d7-8645000102c1865d

Trevino, R.H.V., & Vendeville, B. C. (2008). Origin of coast-perpendicular extensional faults, western Gulf of Mexico: The relationship between an early-stage ridge and a late-stage fault. AAPG Bulletin, 92(7), 951-964. doi:10.1306/03250807070

Whitbread, T., Nicholas, T., & Owens, B. (2001, October). Structural evolution of a detached delta system-the Vicksburg of south Texas. Leading Edge, 1106-1117. doi:10.1190/1.1487240

Whitbread, T., Nicholson, T., Owens, B. (2000). The Vicksburg of South Texas: A Delta System with an Attitude. AAPG Bulletin, 84. https://doi.org/10.1306/8626c32f-173b-11d7-8645000102c1865d

Zhou, L., Han, G., Dong, Y., Shi, Q., Ma, J., Hu, J. (2019). Fault-sand combination modes and hydrocarbon accumulation in Binhai fault nose of Qikou Sag, Bohai Bay Basin, East China. Petroleum Exploration and Development 46, 919–934. https://doi.org/10.1016/S1876-3804(19)60249-1